Homogeneous Dispersion of Magnetic Nanoparticles Aggregates in a PS Nanocomposite: Highly Reproducible Hierarchical Structure Tuned by the Nanoparticles' Size

Anne-Sophie Robbes, Jacques Jestin, Olivier Sandre, Florian Meneau, Florent Dalmas, Javier Perez, François Boué, Fabrice Cousin

To cite this version:

HAL Id: hal-00533476

https://hal.science/hal-00533476

Submitted on 25 May 2019

Figure TOC

Homogeneous Dispersion of Magnetic Nanoparticles Aggregates in a PS Nanocomposite: Highly Reproducible Hierarchical Structure tuned by the Nanoparticles Size.

Anne-Sophie Robbes[1,2], Jacques Jestin[1], Florian Meneau[2], Florent Dalmas[3], Olivier Sandre[4],Javier Perez[2], François Boué[1],Fabrice Cousin[1,]*

[1]Laboratoire Léon Brillouin, CEA Saclay 91191 Gif sur Yvette, Cedex France

[2]Synchrotron SOLEIL, L'Orme des Merisiers, PO Box 48, Saint-Aubin, 91192 Gif sur Yvette, France

[3]Institut de Chimie et des Matériaux Paris-Est, CNRS UMR 7182, 2-8 rue Henri Dunant 94320 Thiais, France

[4]Laboratoire Physicochimie des Electrolytes, Colloïdes et Sciences Analytiques, UMR CNRS-UPMC-Univ Paris 6-ESPCI-Paris Tech 7195, 4 place Jussieu, case 51, 75005 Paris, France

RECEIVED DATE (to be automatically inserted after your manuscript is accepted if required according to the journal that you are submitting your paper to)

[*] Corresponding author: fabrice.cousin@cea.fr

ABSTRACT

We present here the synthesis and structural characterization of new nanocomposites made of spherical magnetic nanoparticles of maghemite (γ-Fe_2O_3) dispersed in a polystyrene (PS) matrix. The γ-Fe_2O_3 nanoparticles, synthetized in aqueous media, were first gently transferred by dialysis in dimethylacetamide (DMAc), a polar solvent which is a good solvent for PS. Electrostatic repulsions enable to keep colloidal stability in DMAc. The nanocomposites were then processed by a controlled evaporation of DMAc of binary mixtures of γ-Fe_2O_3 nanoparticles and PS chains. The size of the nanoparticles ranges from 3.5 to 6.5 nm and can be changed without any modification of the nanoparticles' surface. The structural organization of the nanoparticles inside the polymer was determined as a function of the nanoparticles' size. It was performed by combining very high resolution SAXS measurements which permit to decrease the nanoparticles content down to very low values ($\Phi_{mag} \sim 10^{-5}$) and TEM microscopy. Whatever the size, the nanoparticles are organized with a hierarchical structure that shows that their aggregation has been driven by a two-step process. At low spatial scale, dense primary aggregates composed of some tens of nanoparticles are formed whatever Φ_{mag}, resulting from the first aggregation step. For $\Phi_{mag} > 10^{-4}$, these primary aggregates underwent a second aggregation step and are organized at larger scale in fractal aggregates of finite size of ~ 200nm of radius, with a dimension of 1.7. The size of the dense primary aggregates is almost constant when changing the nanoparticles radius, i.e the mean aggregation number of primary aggregates decreases with an increase of the radius.

I Introduction

The mechanical properties of a polymeric film can be improved by the inclusion of hard particles inside the matrix. In the last two decades, a specific attention has been focused on the reduction of the size of the particles down to the nanometer range to increase the specific surface between the particles and the polymer in order to improve both the reinforcement and the deformability of the resulting materials [1]. From an applicative point of view, the refined understanding of the mechanisms which govern the properties of the filled-polymer system is of great interest in order to design new materials with dedicated and controlled mechanical properties [2]. From a fundamental point of view, one still open question is to correlate the structural and dynamical properties of the components of the system at the microscopic level, i.e. the local structure of the filler and the polymer chain conformation, to the macroscopic response of the material like the elastic modulus. It is now commonly admitted that both the filler structure and chains dynamics contribute to the mechanisms of reinforcement. The contribution of the filler network comes from possible reorganizations under stretching (displacement/rotation, association/dissociation, and reorganization/breaking). It has been extensively studied from simple hydrodynamic models [3] to percolation effects at large filler content [4-7] in the linear, but also in the non linear regime with filler network breakdown and non affinity reorganizations [8]. The contribution of the chains, either before deformation or under stretching, has also been studied by simulations [9] and by experimental approaches [10, 11]. The emerging idea [12] to explain its influence on the reinforcement effects is the existence of a fraction of chains under a "glassy" state which will contribute to the elastic modulus as a rigid phase of the system. However, up to now, the direct measurement of this glassy fraction is still under discussions [13] as both contributions, filler and chains, can be correlated or not under deformation. As a consequence, it is difficult to separate their relative influence on the final properties of the materials at the macroscopic scale. Different strategies have been recently developed to elucidate these mechanisms by decoupling the contributions. Two main strategies are explored: modifying the interactions without changing the filler structure, or changing the polymer-filler

interactions without modifying the filler organization. The first method can be achieved by grafting the filler by the same polymeric chains as the ones of the matrix [14, 15]. It is attractive but implies to develop specific chemistry processes for the grafting of the filler. The second method, that can be achieved by a simpler processing route like simple mixing of components, offers nice perspectives for the design of model systems. Following this idea, some examples can be found using anisotropic or fractal fillers [16, 4] or changing the electrostatic interactions [17]. However, whatever the strategy used, changing the filler morphology at the local scale without changing organization at the large scale inside the polymer matrix by a simple tuning parameter (which is usually the particle content), is difficult because the filler-filler interactions usually depend of the filler concentration.

In the present paper, we present a new model system of filler-polymer nanocomposite that really enables to change the polymer-filler interactions without modifying the filler organization at large scale. It is made of polystyrene (PS) matrix reinforced by spherical magnetic nanoparticles of maghemite (γ-Fe_2O_3). Its specificity comes from the fact that different batches of nanoparticles with various mean radii ranging from 3.5 to 6.5 nm can be obtained starting from a single batch of nanoparticles after using a specific size-sorting process [18] based on colloidal gas-liquid transitions [19]. We thus dispose of a system for which the particle size can be finely tuned without making any surface modification. It provides us a new key parameter to manage the filler structure inside the polymer matrix. Such similar tuning of the particle size in nanocomposites is indeed rather difficult for other mineral particles, like silica for example, as it implies to synthesis each particles size separately, which results in surface modifications that can induce changes in polymer-filler interactions.

 The use of magnetic nanoparticles has also a great potential interest for the improvement of the properties of polymeric systems in further studies. It has been demonstrated in the literature that it is possible to take advantage from the magnetic aspect of nanoparticles to design either magneto-stimulable crosslinked gels [20, 21] or to create controlled anisotropic structures in nanocomposites using a magnetic field during casting [22].

The paper is organized as follow: first we present the analysis of the nanoparticles in solution and especially the transfer from water to an organic solvent, dimethylacetamide, while keeping the colloidal stability using a dialysis process. Second, we have adapted the film processing developed by Jouault et al. [5] for silica fillers to our system in order to form homogeneous nanocomposites. Finally, the structure of the particles inside the polymer matrix is analyzed with a refined combination of high resolution SAXS measurements at the nanometer scale, which permit to cover a large range of particles volume fraction (from 10^{-5} to 5.10^{-2}), with TEM microscopy which enable to validate the structure in the real space and the homogeneity at larger scale. The filler structure is then discussed as a function of the filler content and as a function of the tunable parameter, i.e. the native nanoparticles' size.

II Materials and Methods

II.1 Synthesis of magnetic γ-Fe₂O₃ nanoparticles in aqueous solution

II.1 Synthesis of magnetic γ-Fe$_2$O$_3$ nanoparticles in aqueous solution

The maghemite (γ-Fe$_2$O$_3$) nanoparticles were chemically synthesized in water by coprecipitation in an aqueous ammonia solution of FeCl$_2$ and FeCl$_3$ salts. As a result we obtain colloidal magnetite which is fully oxidized to maghemite by Fe(NO$_3$)$_3$ in acidic medium [23]. The experimental conditions have been chosen in order to prepare particles with an average radius of the order of 40 Å. They have a roughly spherical shape. A size-sorting process based on colloidal gas-liquid transitions allowed then to split up the population of nanoparticles according to their diameter [18]. 4 batches of nanoparticles, with different sizes, have been obtained by such fractionation of the initial suspension. The size of the nanoparticles of the different batches and their volume fraction of magnetic nanoparticles Φ_{mag} were obtained by magnetization measurements performed with a home-made vibrating magnetometer device. The principle of the determination of the distribution of the radii from the magnetization curve [24] is recalled in supporting Information. The sizes were also measured by SAXS (see table 1 in part III).

At the end of the synthesis, the positively charged naked nanoparticles were electrostatically stabilized at pH ~ 2 by HNO$_3^{+-}$ counterions (their PZC is 7.2). The ionic strength was ~ 2 10^{-2} mol/L. The ζ

potential of the nanoparticles, measured on a commercial setup (Delta Nano C, Beckman Coulter, France), was + 60mV.

These synthesis processes enabled us to get large amounts of the different suspensions, as we obtained several hundreds of ml of each batch with a Φ_{mag} higher than 0.02.

- Transfer in DMAC solvent by dialysis

The magnetic nanoparticles were then transferred by dialysis in the dimethylacetamide (DMAc), a polar solvent (ε_r = 37.8) which is also a good solvent for the polystyrene (PS), the polymer used as a matrix for the nanocomposite. The initial aqueous suspension of γ-Fe$_2$O$_3$ nanoparticles was placed in a dialysis bag made of regenerated cellulose with a MCWO Cut-off of 12000-14000 Da (Roth-Sochiel, France). The bag was then placed in a reservoir of DMAc (purity >99.9% %, Sigma Aldrich, France). The dialysis enables to exchange progressively the molecules of the solvent, respectively water and DMAc, while keeping the colloidal stability. The DMAc bath was changed several times to exchange almost all molecules of water. We stopped the procedure of changing bath when such traces of water were low enough in the reservoir to allow the solubilization of chains of highly hydrophobic PS within the solvent.

The ζ potential of the nanoparticles after the transfer was still positive with a value of + 11mV.

- Sample Preparation

The sample preparation process have been developed by Jouault et al. [Jouault 2009] for silica nanoparticles and adapted here to maghemite particles. We use polystyrene (PS, Aldrich, Mw 280000 g/mol, Ip = 2, used as-received) as a matrix. The glass transition T_g of pure PS is around 100 °C. A concentrated solution of PS in DMAc (10% v/v) is mixed with a solution of maghemite nanoparticles previously transferred in DMAc, ranging from 0 to 5% v/v. The mixtures are stirred (using a magnetic rod) for 2 h. They are then poured into an aluminium cup and let cast in an oven at constant temperature T_{cast} = 130 °C during 8 days. At the final stage, the residual solvent content inside the film is below 1%

w/w. This yields spherical dry films of 5 cm of radius and 0.1 cm of thickness (i.e., a volume of 1.9 cm^3).

- SAXS and SANS scattering

The SAXS experiments on the nanocomposites and solutions were carried out at the SWING beamline at Soleil, using a sample changer enabling to load 10 samples simultaneously. SAXS measurements were recorded with the 2D AVIEX CCD camera, placed in the vacuum detection tunnel. 2 setups were used in order to obtain a large q-range. The sample to detector distance was fixed at 6.5m and 1.8m and a beamstop of 3 mm (vertical size) with a photodiode inserted in its center enabled us to measure the transmitted intensity. The experiments at 6.5m were repeated using a specially designed beamstop of 1 mm in order to access very small q values: q_{min}= 4.4 $10^{-4}A^{-1}$. The beamline energy was set to 7 keV for all experiments which enabled to obtain a large q range going from 1.8 10^{-3} to 0.15A^{-1}, where $q=2\pi sin\theta/\lambda$. The parasitic scattering from the air and mica windows was subtracted from the total scattering intensity. The resulting curves were normalized to take into account the effects related to the detector non-linearities and sample transmission. The 2D SAXS images obtained were radially averaged and corrected for the transmitted intensity using Foxtrot, the data reduction and analysis program developed at Soleil. In order to subtract the contribution of the PS chains in the nanocomposite samples, we have measured a pure PS matrix sample without magnetic nanoparticles I_{pure_PS} and subtracted (1-$\Phi_{mag}*I_{pure\_PS}$) from all the nanocomposite samples. Concerning the liquid samples, both the scattering of the solvent $I_{solvent}$ and the capillary $I_{capillary}$ were removed by the subtraction of (1-$\Phi*I_{solvent}-I_{capillary}$) from all the solutions.

 SANS measurements were done on PACE spectrometer at LLB (LLB, Saclay, France). One configuration was used (Sample-Detector = 4.7m; λ = 6 Å), covering a q-range from 7.10^{-3} to 7.10^{-2} Å^{-1}. All measurements were done under atmospheric pressure and at room temperature. Standard corrections for sample volume, neutron beam transmission, empty cell signal subtraction, detector efficiency, subtraction of incoherent scattering and solvent buffer were applied to get the scattered intensities in absolute scale [25].

- Transmission Electronic Microscopy

In order to complete on a larger scale the SAS analysis of the nanocomposite structure, conventional TEM observations were also performed on the composite materials. The samples were cut at room temperature by ultramicrotomy using a Leica Ultracup UCT microtome with a diamond knife. The cutting speed was set to 0.2 mm s^{-1}. The thin sections of about 40 nm thickness were floated on deionized water and collected on a 400 mesh copper grid. Transmission electron microscopy was performed on a Tecnai F20 ST microscope (field-emission gun operated at 3.8 kV extraction voltage) operating at 200 kV. Precise observations of various regions of the sample were systematically done, starting at a small magnification which was then gradually increased. The sections observed were stable under the electron beam. The sample aspect remained similar on the whole area and for all pieces. Except for a few cutting scratches, moderate buckling, very rare bubbles, and impurities, the pictures presented below are completely representative of the single aspect of the sample, which thus appears homogeneous.

## III Obtaining stable binary mixtures of magnetic nanoparticles and PS polymeric chains

1 Transfer and stability of γ–Fe$_2$O$_3$ magnetic nanoparticles in DMAc

It has been demonstrated that DMAc enables a good control of the aggregation of the silica nanoparticles in the PS matrix [5]. Thus the film processing needs a first step of transfer of naked γ-Fe$_2$O$_3$ nanoparticles, initially in water, to the organic medium. However, the transfer of such γ-Fe$_2$O$_3$ nanoparticles in DMAc has never been reported. We present in this section how we achieved it and checked the stability of the nanoparticles by SAXS.

1.1 Structure of acidic aqueous suspensions of γ–Fe$_2$O$_3$ magnetic nanoparticles

Prior to the transfer in DMAc, we have first checked by SAXS the stability of the aqueous suspensions and determined the nanoparticles size for the four batches of particles. These four batches will be denoted hereafter A, B, C and D.

The suspensions were measured at 2 different volume fractions of maghemite nanoparticles Φ_{mag}: immediately after the size-sorting process at $\Phi_{mag} = 0.028$ and a dilute one at $\Phi_{mag} = 0.001$. The initial suspensions were diluted in distilled water. We show the results in Figure 1.a for nanoparticles C. The results for the other batches are very similar and are presented in the Supporting Information (Figures SI.1.a, SI.1.b, SI.1.c).
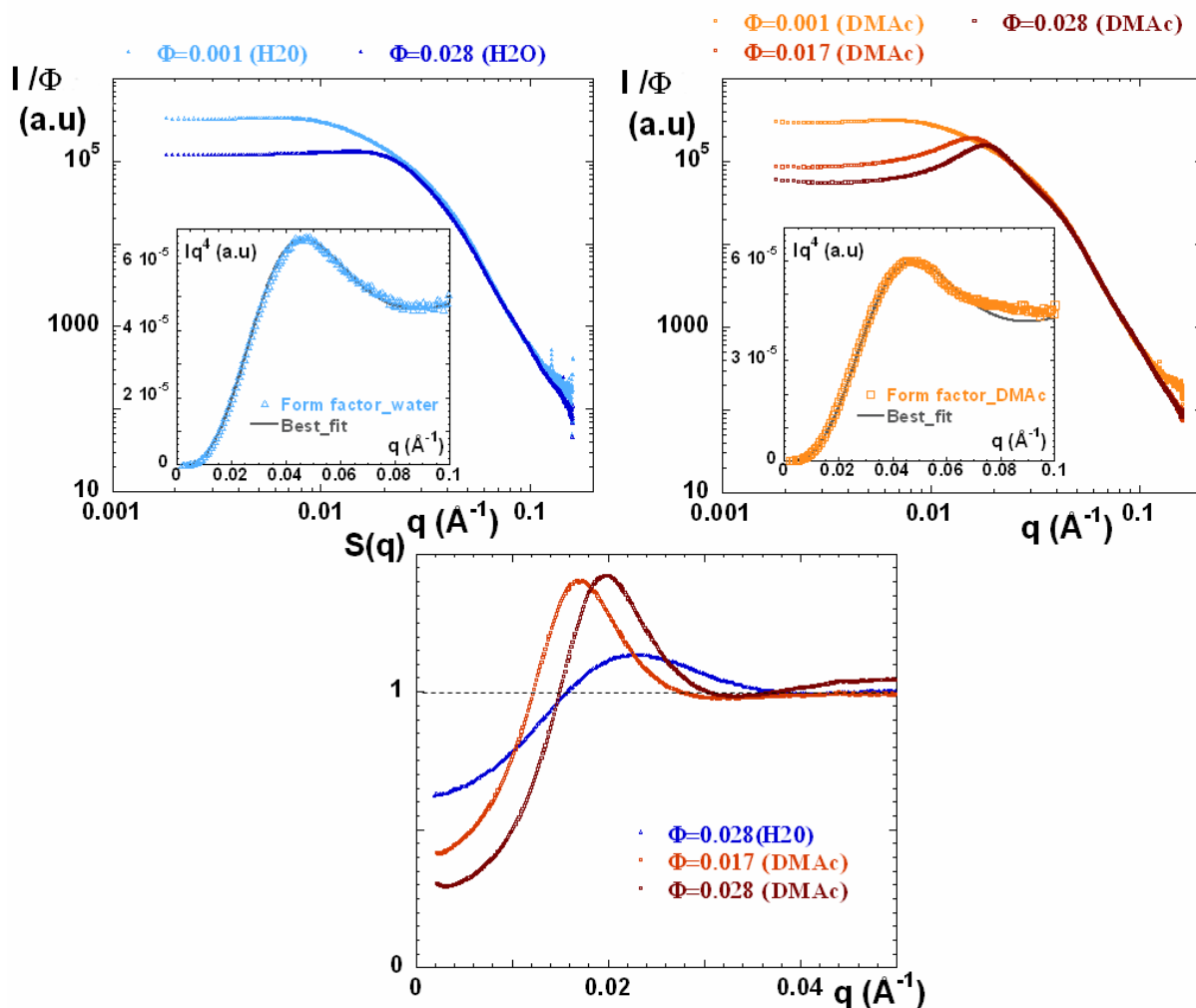
Figure 1: (a) SAXS scattering curves for the suspensions of nanoparticles C in water. Inset: $q^4 I(q)$ versus q for $\Phi_{mag} = 0.001$ in water. The full line corresponds to the best fit of the form factor. (b) SAXS

10

scattering curves for the suspensions of nanoparticles C in DMAc. Inset: $q^4 I(q)$ versus q for Φ_{mag} = 0.001 in DMac. The full line corresponds to the best fit of the form factor. (c) Comparison of the structure factors of the concentrated suspensions of nanoparticles C in water and in DMAc.

Since the spherical nanoparticles are centrosymetrical, their scattering is written as follow:

$$I(q) = \Phi_{mag} (\rho_{mag} - \rho_{solv})^2 V_{NP} P_{NP}(q) S(q) \tag{1}$$

where ρ_{mag} and ρ_{solv} are the respective scattering electronic density of maghemite and solvent (water or DMAc), V_{NP} is the volume of the nanoparticles, $P_{NP}(q)$ their form factor and $S(q)$ the structure factor.

For very dilute solutions, *i.e* when Φ_{mag} = 0.001, we assume that the interactions between the nanoparticles are negligible and thus $S(q)$ is equal to 1 on all the probed q-range. This measurement allows us to determine $P_{NP}(q)$ that gives the size and shape of the nanoparticles. The plateau obtained at low q in the Guinier range (q < 0.01 Å^{-1}) confirms that the interactions between particles can be almost neglected. At large q (q > 0.06 Å^{-1}) in the so-called Porod regime, $I(q)$ roughly decreases like q^{-4}, which is characteristic of solid particles with a sharp interface. No oscillations are obtained in the form factor, indicating that the size distribution of the complexes is polydisperse. $P_{NP}(q)$ is modelled by the form factor of a sphere with a lognormal distribution of median radius R_0 and polydispersity σ :

$$V_{NP} P_{NP}(q) = \frac{\int_0^\infty \frac{4}{3} \pi R^3 \left(3 \frac{\sin(qR) - qR\cos(qR)}{(qR)^3} \right)^2 R^3 P(R) dR}{\int_0^\infty R^3 P(R) dR} \text{ with } P(R) = \frac{1}{\sqrt{2\pi}\sigma R} \exp\left[-\frac{1}{2\sigma^2} \left(\ln\frac{R}{R_0} \right)^2 \right] \tag{2}$$

The mean diameter of the nanoparticles R_{NP_mean} is obtained from $R_{NP\_mean}^3 = R_0^3 e^{\frac{9}{2}\sigma^2}$. The best fit is presented in the inset of Figure 1, in a $I(q)q^4 = f(q)$ representation. A maximum appears at a q position which is directly linked to the average radius of the spheres. R_0 and σ can be unambiguously determined because R_0 is linked to the peak q-position and σ to the adjustment of the shape of the peak. The results

11

for all sizes are presented in Table 1. They are compared with the ones obtained from magnetization measurements. The magnetization curves are presented in Figure SI.2 of the Supporting Information. Results from the two techniques are in excellent agreement. The four batches have close polydispersities and different R_{NP_mean} ranging from 37 Å to 65 Å, proving that the size-sorting process has been successful.

	R_0 (Å) ; σ (SAXS)	R_0 (Å) ; σ (magnetization)	R_{NP_mean} (Å) (SAXS)
A	32 ± 1; 0.32	33 ± 1; 0.29	37 ± 2
B	38 ± 1 ; 0.32	38 ± 1; 0.32	45 ± 2
C	44 ± 1 ; 0.32	45 ± 1; 0.27	51 ± 2
D	54 ± 1 ; 0.32	52 ± 1; 0.34	65 ± 2

Table 1: Size characteristics of the different batches γ-Fe$_2$O$_3$ nanoparticles obtained by SAXS and magnetization measurements.

The scattering curves of the suspensions for the dilute and concentrated volume fractions superimpose at large q in the Porod regime ($I(q)/\Phi\Delta\rho = f(q)$) to the one at Φ_{mag} = 0.001. This is due to the fact that only the form factor is probed in the Porod regime. However, for Φ_{mag} = 0.028, the scattering curve has a different behavior at low q. It presents a soft maximum around 0.02 Å^{-1}.This comes from the inter-particle interactions which are no longer negligible and the structure factor $S(q)$ in equation (1) is no more equal to 1. This structure factor is presented in Figure 1.c. It is calculated by dividing the total scattering by the form factor of the nanoparticles. It is equal to 1 at large q, it shows a correlation peak at intermediate q and it tends to a value inferior to 1 when q → 0. In the thermodynamic limit (for q → 0), it tends to the isothermal osmotic compressibility of the system. Its decay to a value inferior to 1 when going towards very low q means that the interparticle interactions are repulsive on average. The

nanoparticles must thus be homogeneously dispersed in the suspension and the correlation peak of the structure factor at q^* ~ 0.022 Å^{-1} should correspond in real space to the mean interparticle distance between the nanoparticles d_{mean}. In this case, $2\pi/q^*$ must be equal to $d_{mean} = (2R_{NP\_mean})^3 \sqrt{\dfrac{\pi}{6\Phi_{mag}}}$ as Φ_{mag} = $V_{NP\_mean}^3/d_{mean}^3$. For Φ_{mag} = 0.028, one gets d_{mean} = 285 Å from the measurement (q_{max} ~ 0.022 Å^{-1}) and 272 Å from the calculation. The excellent agreement between those two estimations confirms the perfect dispersion of the nanoparticles.

These results are in agreement with the values of the 2nd Virial coefficients of similar suspensions obtained by osmotic measurements [26]. In such suspensions of naked (γ-Fe$_2$O$_3$) nanoparticles in aqueous acidic medium, there are three main interactions that contribute to the interparticular potential [26, 27]: (i) short-range Van der Waals attractions, (ii) magnetic dipolar interactions, which are found to be globally attractive if the anisotropic interparticle potential is integrated over all directions. They vary from -1/r^6 to -1/r^3 depending on the strength of the magnetic coupling $\gamma = (\mu_0/kT)(\mu_1\mu_2/r^3)$ between two nanoparticles of respective momentum μ_1 and μ_2. Finally there are (iii) the coulombian electrostatic repulsions at longer range described by a Yukawa potential according to the DLVO theory [28] :

$$\frac{V_{el}(r)}{kT} = \frac{Z_{NP}^2 e^2}{4\pi\varepsilon_r\varepsilon_0 k_B T}\frac{e^{-\kappa r}}{r} \text{ where } \kappa = \sqrt{\frac{2e^2 I}{\varepsilon_r\varepsilon_0 k_B T}} \tag{3}$$

where Z_{NP} is the number of charges carried by the nanoparticles, e the elementary charge of an electron, ε_0 the permittivity of the vacuum, ε_r the relative permittivity of the medium (78.5 in water), k_B the Boltzmann constant, T the temperature, κ the inverse of the Debye length and I the ionic strength defined by $I = \frac{1}{2}\sum_i c_i z_i^2$ (c_i is the concentration of the ionic specie i and Z_i its valency).

In our experimental conditions at pH 2, the surface of the nanoparticles is strongly positively charged as its ζ potential equals + 60 mV. As a result the coulombic repulsions are sufficiently important to overcome the attractive interactions at moderate ionic strength. As shown in Figure S.I 1 in Supporting Information, the sum of the interactions in all the aqueous suspensions from the different batches is

always repulsive, even for the largest nanoparticles D, although the attractive interactions strongly increase with size.

1.2 Structure of the suspensions of γ–Fe_2O_3 magnetic nanoparticles in DMAc

After the solvent transfer of the naked (γ-Fe_2O_3) nanoparticles, the interparticular potential is much more repulsive in DMAc than in water because the soft maximum associated to the correlation peak of the structure factor is much marked, as shown by the SAXS scattering curves of Figure 1.b. This is highlighted in Figure 1.c which compares the structure factor at Φ_{mag} = 0.028 in DMAc to the one at Φ_{mag} = 0.028 in water. The correlation peak at q^* is much more pronounced as it reaches a value of 1.4 in DMAc while it was around 1.15 in water. Accordingly, the isothermal osmotic compressibility has been strongly reduced because $S(q)_{q \to 0}$ tends to a much lower value.

We have also checked that a dilution in pure DMAc of the suspension after dialysis does not affect its stability by comparing in figure 1.c the structure factor of a suspension at Φ_{mag} = 0.017 with the one at Φ_{mag} = 0.028. Both structure factors look very similar. As d_{mean} increases with dilution, the correlation peak is shifted towards low q. The height of the correlation peak is slightly lower for Φ_{mag} = 0.017. $S(q)_{q \to 0}$ has a higher value for Φ_{mag} = 0.017, in accordance with the fact that the isothermal osmotic compressibility decreases when increasing Φ_{mag}, in a case of repulsive interparticle interactions on average. At very low Φ_{mag}, please note that the form factor of the nanoparticle is the same after the transfer in the organic solvent.

In DMAc, the attractive interactions in the system are close to the ones in water. The magnetic dipolar interactions, that depend only on R_{NP_mean}, are exactly similar while the Van der Waals attractions are of the same order (the Hamaker constant is slightly changed because the relative permittivity of DMAc is around twice lower than the one of water). The strong changes in the interparticular potential are thus related to an important increase of the electrostatic repulsions. The nanoparticles indeed still bear a positive charge because the ζ potential was still measurable at + 11 mV. The high dielectric constant of

DMAc enables the dissociation of the Fe-OH groups at the nanoparticles surface. The surface charge of the nanoparticles has nevertheless been strongly reduced compared to the acidic aqueous suspension as ζ was reduced from + 60 mV down to +11 mV. However the dialysis procedure with several baths in pure DMAc had progressively washed away all ions and the ionic strength I at the end of the transfer is close to 0 (only the nanoparticles counterions ensure the electroneutrality of the suspension). Thus, during the transfer process, the strong reduction of I combined with the decrease of ε_r overcompensate the decrease of Z_{NP}, which globally increase the electrostatic repulsions. Please note that the elimination of the ionic strength by the use of dialysis to transfer the solvent is crucial. We tried to exchange the solvents by evaporating the water on mixtures of acidic aqueous suspensions and DMAc by simple boiling. It always leads to flocculation during the process because the salt was not removed but progressively concentrated.

As for the aqueous suspensions, we checked that the sum of the interactions of the suspensions with the four different sizes of nanoparticles in DMAc was repulsive (see Figure S.I 1 in Supporting Information).

2 Effect of the addition of PS chains on the suspensions of γ–Fe₂O₃ magnetic nanoparticles in DMAc

Prior to the processing of the films, we have studied the influence of the addition of a large amount of PS chains on the colloidal stability of γ-Fe$_2$O$_3$ nanoparticles suspensions in DMAc. We have measured by SANS the scattering of a suspension of nanoparticles C at Φ_{mag} = 0.015 in which we added a quantity of PS chains (10% v/v). The scattering signal of the PS chains was matched to get only the scattering of the maghemite nanoparticles. The measurements were performed in a mixture of 15% of deuterated DMAc (Euristop France) and 85 % of hydrogenated DMAc which has a neutron scattering length density $\rho_{mixture}$ of 1.43 10^{-10} cm^{-2} that exactly matches the one of hydrogenated PS. The nuclear scattering length density of maghemite $\rho_{\gamma\text{-Fe2O3}}$ has a very different value (6.96 10^{-10} cm^{-2}), which enabled a measurement of the scattering of the nanoparticles alone with a good statistics.

15

The scattering intensity of the maghemite nanoparticles in the DMAc suspension with contrast-matched PS chains is presented in the inset of Figure 2. It can be described as presented in Equation 1, by a product of a form factor and a structure factor. The structure factor is displayed in figure 2 where it is compared to the one of a suspension with a close Φ_{mag} (0.017) in pure DMAc solution presented in previous section.
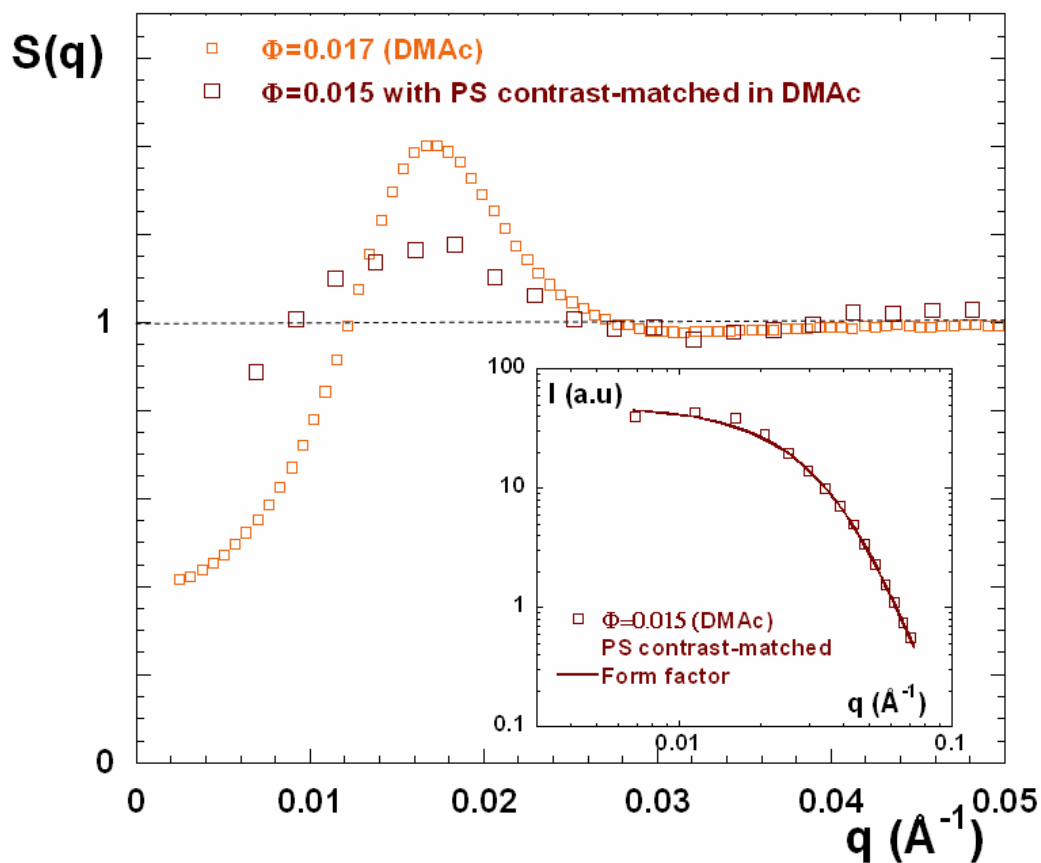

Figure 2: Comparison of the structure factors of the suspensions of nanoparticles C with close Φ_{mag} either in pure DMAc solution or with 10% v/v of contrast-matched PS chains. Inset: SANS scattering of suspensions of nanoparticles C with $\Phi_{mag} = 0.015$ in DMAc with 10% v/v of contrast-matched PS chains. The full line corresponds to the form factor.

It clearly appears that the introduction of the PS chains has changed the interparticular potential between the nanoparticles in the system. The two structure factors have the characteristic features of

repulsive systems ($S(q)_{q \to 0} < 1$ and a correlation peak at intermediate q) with rather similar concentrations. For the suspension with contrast-matched PS chains, q^* is slightly shifted towards the low q compared to the suspension in pure DMAc because Φ_{mag} is slightly lower (0.015 versus 0.017). However, the repulsions are much less marked when PS chains are introduced in solution. The height of the correlation peak at q^*, directly linked to the intensity of the repulsions, decreases from a value of ~ 1.4 in pure DMAc to a value of ~ 1.15 with 10%v/v of PS chains. Accordingly, the isothermal osmotic compressibility is higher as $S(q)_{q \to 0}$ increases from a ~ 0.4 in pure DMAc up to ~ 0.8 with the PS chains.

As the nanoparticles are still in repulsive regime when PS chains are introduced, there are thus no specific interactions between the naked maghemite nanoparticles and PS which would have led to aggregation via a bridging process. The change in the interparticular potential can result from the following changes in the effective interactions between nanoparticles. First, as the content of PS chains is very important, the effective dielectric constant of the binary mixture of DMAc and PS chains is reduced compared to the one of the pure DMAc because $\varepsilon_r \sim 3$ for PS. This can both increase the Van der Waals attractions and decrease the electrostatic repulsions by changing the dissociation of the charges at the surface of the naked nanoparticles. Second, the presence of the PS chains can induce some depletion attractive interactions. However these depletion attractions must have a very limited range. As the PS chains are in semi-dilute regime with a very high concentration, the typical size of the system is the mesh size of the blob ξ of the semi-dilute solution, around 11Å here [29]. The range of the depletion interactions is thus necessarily lower than such a value.

Despite the reduction of the effective repulsions between the nanoparticles in presence of PS chains, our experimental system proves to be a good candidate for forming a nanocomposite with controlled aggregation due to its weak repulsive structure prior to the drying.

IV Structures of aggregates of magnetic nanoparticles in nanocomposites polymeric films

Several nanocomposite films were obtained for the four different types of nanoparticles and over a large range of Φ_{mag} (calculated in this section after evaporation of the DMAc solvent) on almost four decades ranging from 10^{-5} up to 0.05. The films had a surface of $\sim$ 80 cm^2 and a typical thickness ranging from 0.5 to 1 mm. Their aspect was macroscopically homogeneous. As the maghemite optically absorbs in the red, the films diluted in γ−Fe$_2$O$_3$ nanoparticles were red/orange while the most concentrated were black. As reported on the system close to this one, made of silica nanoparticles dispersed in PS matrix [5], there were microcracks at the surface of the films. We describe in this section how we obtained the main structure of the aggregates of γ−Fe$_2$O$_3$ nanoparticles by SAXS and TEM microscopy first by focusing on a single nanoparticle size (sample C) and in a second step, how a change of the initial size of the nanoparticles tunes the aggregation. X-rays scattering is mainly dominated by the contrast between the inorganic particles and the polymer. It directly depends on the particles' concentration in the polymer matrix. Only the powerful high resolution available in the setup of a SAXS apparatus in the synchrotron source enables to determine the structure of filled nanocomposites at the very low nanoparticle content range probed here.

1 Typical features of the scattering of γ−Fe₂O₃ nanoparticles in the nanocomposites polymeric films

We present in this section the main features of the scattering curves of the γ−Fe$_2$O$_3$ nanoparticles within the polymeric matrix obtained by SAXS. They are shown in Figure 3 for the nanoparticles C for

Φ_{mag} ranging from 10^{-5} to 0.05.

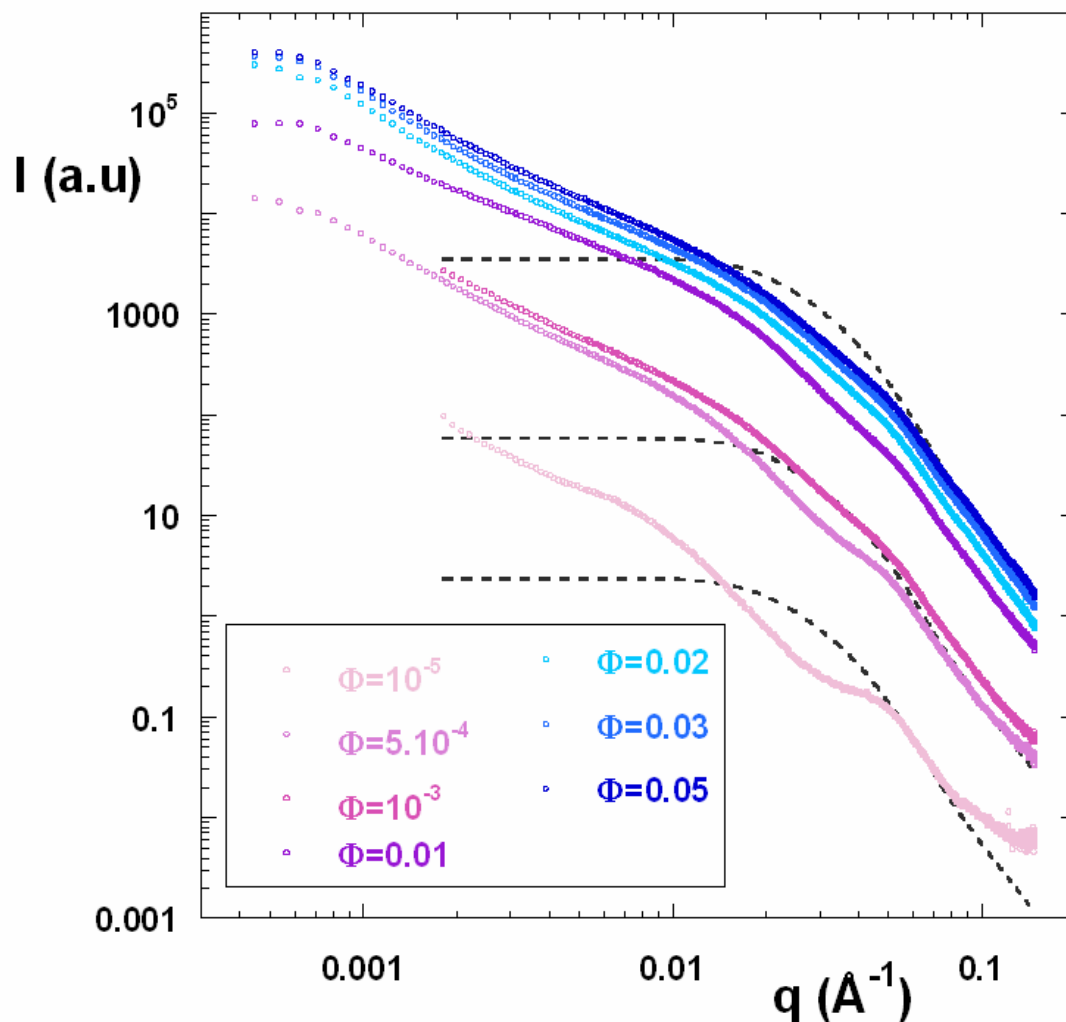Figure 3: SAXS scattering curves of the $\gamma-Fe_2O_3$ nanoparticles in the PS polymeric matrix obtained by SAXS for nanoparticles C. The dashed lines correspond to the form factor of the nanoparticles.

Irrespective of the nanoparticles size and Φ_{mag}, all the scattering curves present a q^{-4} decay at large q (q > 0.1 Å^{-1}) corresponding to the surface scattering of the individual nanoparticles. All the scattering curves perfectly superimpose to the form factors of the nanoparticles measured in section III.1.

At lower q, two distinct behaviors appear depending on Φ_{mag}:

- For $\Phi_{mag} \leq 10^{-4}$, there is a correlation peak in the range 0.05 Å^{-1} - 0.08 Å^{-1}. Its q-position corresponds exactly to $2\pi/(2R_{NP\_mean})$, *i.e* to the contact between 2 nanoparticles in real space. At lower q, the scattering presents a strong decay (between q^{-3} and q^{-4}) and bends toward a Guinier regime around q ~ 0.008 Å^{-1}, indicating that the aggregates have a finite size. At lower q, depending on the samples, there is eventually an upturn at very low q with a q^{-3} behavior.

- For $\Phi_{mag} \geq 5 \ 10^{-4}$, the scattering spectra look different. The correlation peak still exists in the range $5 \ 10^{-3} < \Phi_{mag} < 10^{-2}$ but less pronounced. For higher Φ_{mag}, it is also present but looks more like a break of slope. At intermediate q, the scattering increases rather strongly again and, around 0.025 Å^{-1}, there is a net break of slope for all samples and all Φ_{mag}. The scattering decays like q$^{-1.7}$ (in the q- range 0.0008 Å^{-1} - 0.008 Å^{-1}). At very low q, (q < 0.0008 Å^{-1}), the scattering tends towards a Guinier regime, indicating that the aggregates have a finite size.

This first qualitative description indicates that the overall size of the aggregate is much larger in the high Φ_{mag} regime than in the low Φ_{mag} one, because the Guinier regime is reached at much lower q. As the correlation peak is present for all Φ_{mag}, with a q-postion corresponding to two nanoparticles in close contact, it is likely that the aggregates present at low Φ_{mag}, that will be named hereafter 'primary aggregates', are in fact present for all Φ_{mag}. They must then form aggregates of primary aggregates at higher Φ_{mag} that we will describe in the following by 'supra-aggregates'. We present in the next sections a quantitative analysis of the structure of the supra-aggregates realized in the framework of such a hypothesis.

2 Structure of supra-aggregates from the combined analysis of SAXS scattering and TEM experiments

2.1 Nanocomposites at $\Phi_{mag} \leq 10^{-4}$: Scattering of primary aggregates

Concerning the primary aggregates, the intensity of the correlation peak at $q_{peak} = 2\pi/(2R_{NP\_mean})$ indicates that the contact distance between two nanoparticles is strongly favored in the sample. The primary aggregate must thus be composed of dense clusters of several nanoparticles. This is confirmed in Figure 4.c that presents a TEM picture of such a primary aggregate obtained with nanoparticles C at $\Phi_{mag} = 10^{-5}$. This picture is representative of the aggregates that are observed on the whole TEM grid with a very low content. This explains why the scattering decay of the primary aggregate at intermediate q lies between q^{-3} and q^{-4}, as one probes the surface scattering of a dense object. The Guinier regime at low q and the decay at intermediate q can thus be described by the form factor of polydisperse spheres.

However this does not explain the q^{-3} upturn observed at very low q. It could arise from the presence of a limited number of larger aggregates but none are observed on the whole TEM grid (Figure 4.c). The q^{-3} upturn indeed comes from the scattering of microcracks present in the sample, which decay like q^{-3}, as it as been shown in [30]. Even after the subtraction of the pure PS matrix (see the Materials and Methods section), there remains some scattering signal of microcracks because their scattering behavior is modified by the presence of the nanoparticles. At low q, the whole scattering can thus be described by the linear combination of a form factor of polydisperse spheres and of a q^{-3} decay with a K prefactor:

$$I(q) = \Phi_{mag}(\rho_{mag} - \rho_{PS})^2 \frac{\int_0^\infty \frac{4}{3}\pi R^3 \left(3\frac{\sin(qR) - qR\cos(qR)}{(qR)^3}\right)^2 R^3 P(R)dR}{\int_0^\infty R^3 P(R)dR} + Kq^{-3} \qquad (4) \qquad \text{where}$$

P(R) accounts for the same lognormal law as in equation (2). However, the median radius is here the one of the primary aggregate R_{PA_0}. Accordingly, we deduce the mean radius of the primary aggregates R_{PA_mean} from $R_{PA\_mean}{}^3 = R_{PA\_0}{}^3 e^{\frac{9}{2}\sigma^2}$.
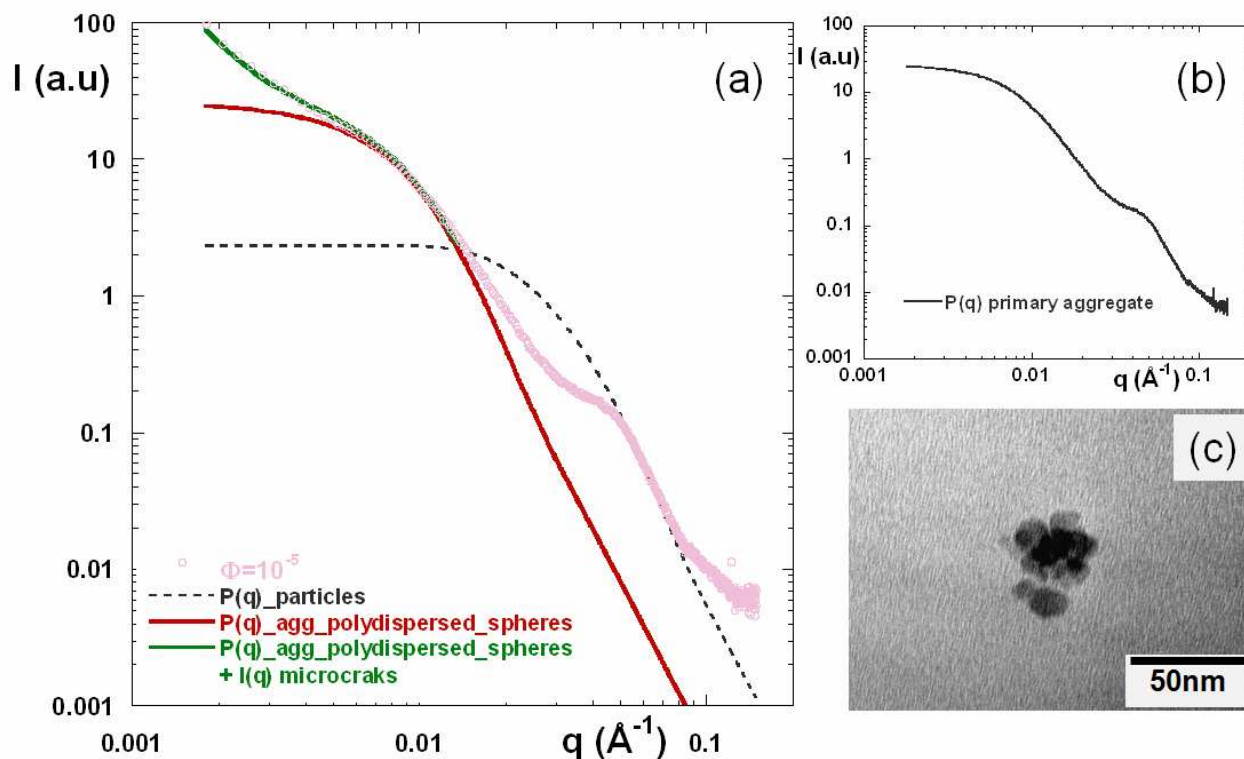
Figure 4: (a) Scattering of primary aggregates of nanoparticles C at $\Phi_{mag} = 10^{-5}$, decomposed at low q in a linear combination of the form factor of polydisperse spheres and scattering of microcracks, compared with the form factor of the nanoparticles C at the same Φ_{mag}. (b) Scattering of the form factor of primary aggregates of nanoparticles C. (c) TEM picture of a nanocomposite made of nanoparticles C at $\Phi_{mag} = 10^{-5}$.

It is shown in Figure 4.a how such a linear combination enables to perfectly modeled the low q scattering of the primary aggregate of nanoparticles C measured at $\Phi_{mag} = 10^{-5}$ (for q < 0.02 Å^{-1}). In the next sections, the form factor of the primary aggregate of nanoparticles C will be described by such a scattering curve after the subtraction of the microcracks scattering. It is shown in Figure 4.b.

The mean radius of the primary aggregate R_{PA_mean} is 168 Å (R_{PA_0} = 140 Å; σ = 0.35), about three times the mean diameter of the nanoparticles, in accordance with Figure 4.c.

As the scattering of an assembly of non-interacting centro-symmetrical objects can be described by equation 1, with S(q) = 1 for all q, the value of $I_{objects}(q=0)/\Phi\Delta\rho^2$ is a direct measurement of the volume of the object. This is true both for primary aggregates and for isolated nanoparticles. The direct comparison of the scattered intensity of primary aggregates $I_{PA}(0)$ and of the scattered intensity of nanoparticles $I_{NP}(0)$, for same Φ and $\Delta\rho^2$ as shown in Figure 4.a, enables the measurement of the mean number of aggregation in the primary aggregates N_{PA_agg} because $I_{PA}(0) = N_{PA\_agg} I_{NP}(0)$. We obtain $N_{PA\_agg} \sim 10$ for the primary aggregate of nanoparticles C measured at $\Phi_{mag} = 10^{-5}$, here again in accordance with picture of Figure 4.c.

Finally, we can measure the compactness of the primary aggregates because the inner volume fraction of nanoparticles within the primary complexes Φ_{PA_inner} is obtained from:

$$\Phi_{PA\_inner} = N_{PA\_agg}\left(\frac{R_{NP\_mean}}{R_{PA\_mean}}\right)^3 \tag{5}$$

We get $\Phi_{PA\_inner} = 0.3$. This high value confirms that the primary aggregates are dense clusters and explains why they scatter at low q like dense polydisperse spheres.

It is worth noting that a similar scattering behavior of dense clusters of few nanoparticles has also been reported by Fresnais et al [31] on different systems of polymer/inorganic nanoparticles co-assemblies. Although there is no analytic form for the scattering signal of such dense small clusters made of polydisperse spheres, the authors have shown that the scattering features of such clusters can be perfectly recovered by reverse Monte-Carlo simulations.

2.2 Nanocomposites at $\Phi_{mag} \geq 5\ 10^{-4}$: Scattering of supra- aggregates

We detail here the scattering of the supra-aggregates made of primary aggregates. First of all, let us note that the scattering of the microcracks is here negligible compared to the one of the supra-aggregates because Φ_{mag} is rather high. As the primary aggregates are dense 3-D objects, they are centro-symmetrical. The scattering of the supra-aggregates can thus be described like in equation 1 by the

product of the form factor of the primary aggregates and an effective structure factor between primary aggregates $S_{eff}(q)$. The $S_{eff}(q)$ are plotted in Figure 5.a for nanoparticles C at various Φ_{mag} ranging from $5\ 10^{-4}$ to $5\ 10^{-2}$. They are calculated by dividing the scattered intensity by $P(q)_{prim\_agg}\Phi_{prim\_agg}/\Phi_{mag}$, where $P(q)_{prim\_agg}$ is the form factor of the primary aggregate presented in Figure 4.b and Φ_{prim_agg} its volume fraction.
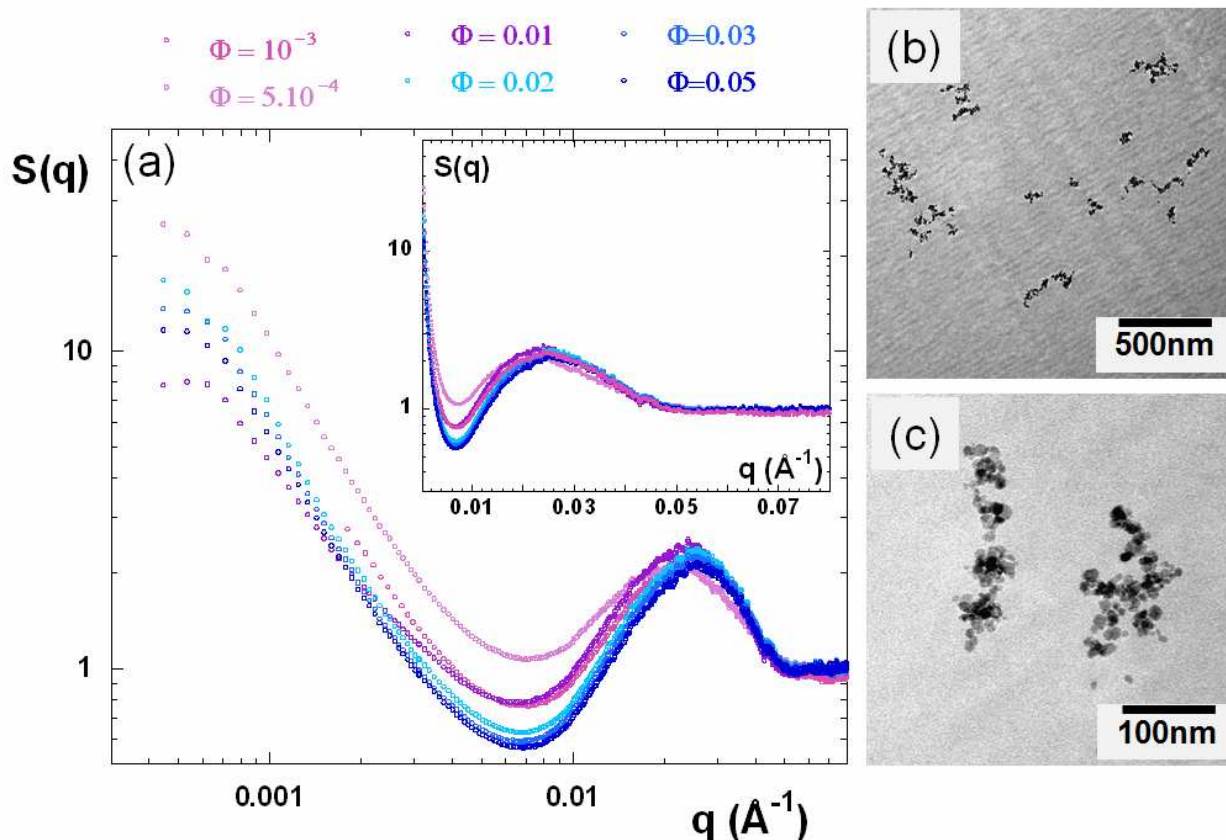

Figure 5: (a) Effective structure factor between the primary aggregates $S_{eff}(q)$ for nanoparticles C. Inset: same $S_{eff}(q)$ in log-linear scale. (b) TEM picture of a nanocomposite made of nanoparticles C at $\Phi_{mag} = 5\ 10^{-4}$. (c) TEM picture of a nanocomposite made of nanoparticles C at $\Phi_{mag} = 5\ 10^{-4}$ with a higher magnification.

Very nicely, $S_{eff}(q)$ is perfectly equal to 1 between 0.05 Å^{-1} and 0.08 Å^{-1} (see inset of Figure 5.a), in the q-region where the correlation peaks were observed (its q-value was 0.06 Å^{-1}). It proves that the mean number of aggregation of primary aggregates N_{PA_agg} is exactly the same at every Φ_{mag} from 10^{-5}

up to $5 \ 10^{-2}$. It validates the hypothesis of supra-aggregates formed by a hierarchical structure made of dense primary aggregates and organized at a higher scale in a more open way.

At lower q, $S_{eff}(q)$ shows a strong correlation peak at $0.025 \ \text{Å}^{-1}$. It roughly corresponds, in real space, to twice the mean radius of primary aggregates. This confirms again the hierarchical structure of the supra-aggregates with primary aggregates in close contact. In figure 3, the slope break observed in this q-range comes from the convolution of such correlation peak in $S_{eff}(q)$ with the form factor of the primary aggregates that is still increasing when going towards low q.

In the q-region ranging from $0.0008 \ \text{Å}^{-1}$ to $0.008 \ \text{Å}^{-1}$, $S_{eff}(q)$ decays like $q^{-1.7}$. The primary aggregates are organized within the supra-aggregates in a fractal way with a fractal dimension D^f of 1.7. Finally, at very low q, the scattering curves reach a Guinier regime. The supra-aggregates have a finite size. All of these features are observed in Figure 5.b and Figure 5.c showing TEM pictures of isolated supra-aggregates measured for nanoparticles C at $\Phi_{mag} = 5 \ 10^{-4}$ with different magnifications.

The SAXS scattering enables to extract quantitative information on the supra-aggregates. In a similar way as we obtained the mean number of aggregated nanoparticles within the primary aggregates N_{PA_agg} in previous section, it is possible to obtain the mean number of aggregated primary aggregates within the supra-aggregates $N_{SA\_PA\_agg}$. The scattered intensity of supra-aggregates $I_{SA}(0)$ is compared to the one of the primary aggregates $I_{PA}(0)$. $N_{SA\_PA\_agg}$ can be directly obtained from Figure 5.a because it corresponds to $S_{eff}(q)$ when $q \rightarrow 0$. We get here $N_{SA\_PA\_agg} \sim 12 - 16$ for Φ_{mag} higher than 10^{-2} and a slightly larger value for $\Phi_{mag} = 5 \ 10^{-4}$. The mean number of total aggregation of nanoparticles within the supra-aggregates N_{SA_agg} is the product of N_{PA_agg} and $N_{SA\_PA\_agg}$. It is ~ 100 for nanoparticles C. In the TEM pictures of Figure 5.b and 5.c, the supra-aggregates seem to contain less nanoparticles than we obtained from SAXS analysis. It is a misleading effect from TEM microscopy because the overall size of the supra-aggregates is larger than the thickness of the cut of the samples used (40 nm, see Materials and Methods section).

The values of D^f, $N_{SA\_PA\_agg}$ and R_{PA_mean} enable to get the mean radius R_{SA_mean} of supra-aggregates:

$$R_{SA\_mean} = N_{SA\_PA\_agg}^{1/D^f} R_{PA\_mean} \tag{6}$$

We obtain $R_{SA\_mean} \sim 800$ Å, similarly as observed in Figure 5.c.

As recalled in the Introduction section, one of the main dominant effects in the reinforcement mechanisms of nanocomposites is the network effect. It is thus important to be able to determine precisely the percolation threshold volume fraction in our nanocomposites. This can be done because all the structural dimensions of the system are quantitatively characterized. Let us determine the effective volume fraction occupied by spheres Φ_{SA} with the radius of supra-aggregates R_{SA_mean} as a function of Φ_{mag} :

$$\Phi_{SA} = \frac{\Phi_{mag}}{N_{SA\_agg}} \left(\frac{R_{SA\_mean}}{R_{NP\_mean}} \right)^3 \qquad \text{or} \qquad \Phi_{SA} = \frac{\Phi_{mag}}{\Phi_{PA\_inner}} N_{SA\_PA\_agg}^{(3/D^f - 1)} \tag{7}$$

For the suspensions of nanoparticles C at $\Phi_{mag} = 0.02$, $\Phi_{mag} = 0.03$ and $\Phi_{mag} = 0.05$, one obtains respectively $\Phi_{SA} = 0.60$, $\Phi_{SA} = 0.79$ and $\Phi_{SA} = 1.2$.

If the supra-aggregates are homogeneously dispersed at large scale, the percolation threshold volume fraction is located at $\Phi_{SA} \sim 1$ when interpenetration between supra-aggregates is forced. The connectivity transition must thus be located at a Φ_{mag} slightly higher than 0.03.

2.3 Homogeneity of supra-aggregates at large scale

In order to know if the supra-aggregates are homogeneously dispersed at large scale, we have taken TEM pictures of films made of nanoparticles C at rather high Φ_{mag} ranging from 0.01 to 0.05. They are presented in Figure 6. For all the Φ_{mag}, we observe a homogeneous dispersion of supra-aggregates with the same structural characteristics as the ones derived from the SAXS analysis of previous section. Several scans of various regions of the samples were systematically done and they show perfectly reproducible pictures over the whole TEM grid. The supra-aggregates are homogeneously dispersed in the whole PS matrix.
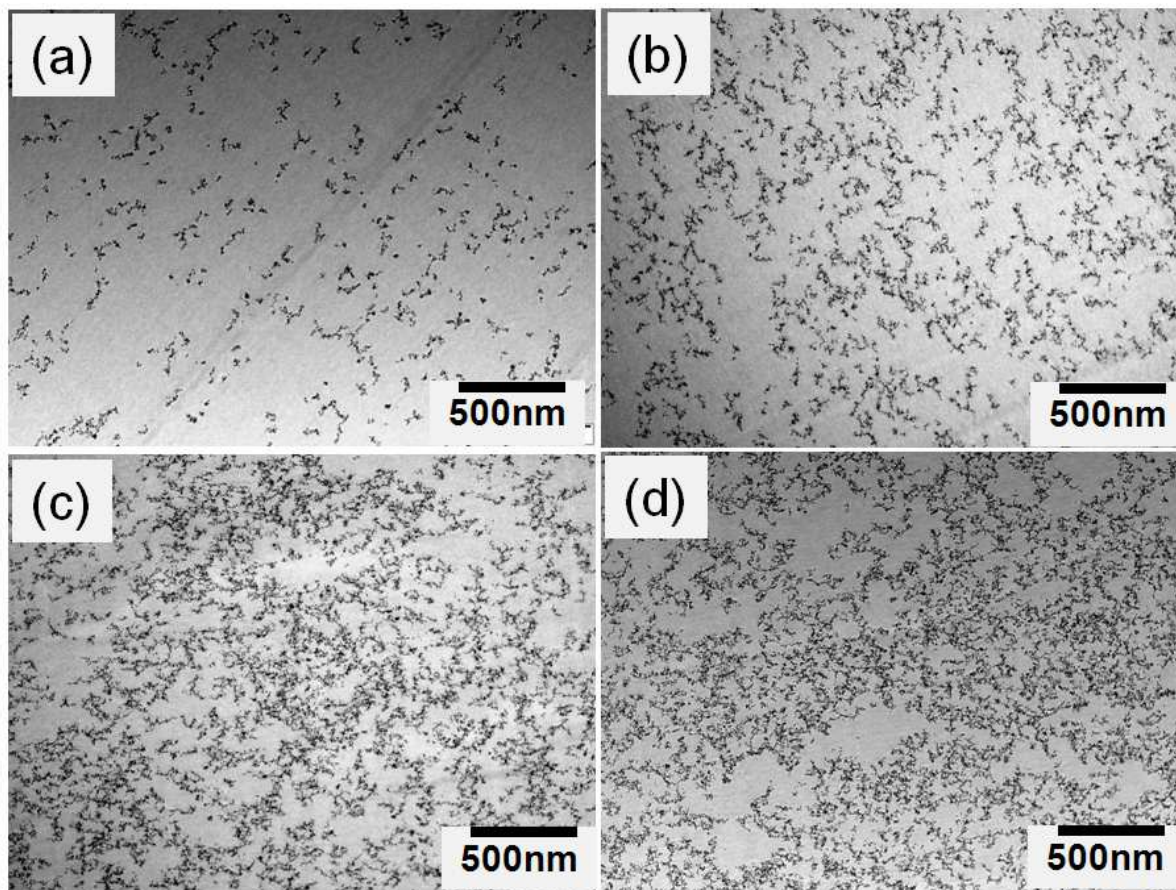
Figure 6: TEM picture of a nanocomposite made of nanoparticles C: (a) Φ_{mag} = 0.01; (b) Φ_{mag} = 0.02;

(c) Φ_{mag} = 0.03; (d) Φ_{mag} = 0.05.

The progressive concentration of the supra-aggregates, by increasing Φ_{mag}, seems to lead to the

percolation of the system between around Φ_{mag} = 0.03, which is in perfect accordance with the previous

SAXS analysis.

3 Influence of the effect of nanoparticles size on the structure of supra-aggregates.

We describe in this part the influence of the nanoparticles' size on the structure of the supra-aggregates.

The SAXS scattering curves for the nanoparticles A, B, and D look very similar to the ones of

nanoparticles C for the whole range of volume fractions. They are presented in Figure SI.3 in Supporting

Information. This shows that the aggregates within the nanocomposites films are produced with a highly

reproducible structure for all nanoparticles' size. There exist nevertheless some differences in the

structure from one size to another. We compare here the scattering of the four different batches in the three regimes of interest: (i) at $\Phi_{mag} = 10^{-5}$ where only the primary aggregates are formed, (ii) at $\Phi_{mag} = 5 \ 10^{-4}$ where the supra-aggregates are formed, far below the percolation threshold, and (iii) at $\Phi_{mag} = 0.03$, close the percolation threshold.

We start first with nanocomposites polymer films diluted in nanoparticles, *i.e* where only the primary aggregates are formed. Figure 7 presents the scattering curves features for the four batches of nanoparticles. As expected, the position of the correlation peak corresponding to the contact of two nanoparticles at $q^* = 2\pi/(2R_{NP\_mean})$ is shifted towards the low q when R_{NP_mean} increases. However, the structure is different from one sample to another. The intensity of the correlation peak changes with the nanoparticles' size. It almost vanishes for nanoparticles D, meaning that the mean number of aggregation in the primary aggregates N_{PA_agg} decreases when the particles size decreases. This comes from the fact that, very nicely and very surprisingly, the mean radius of the primary aggregate R_{PA_mean} is similar for the four sizes of nanoparticles. The shape of the scattering part curves corresponding to the Guinier regime of the form factor of the primary aggregate is indeed similar for all samples, as highlighted by the guide of the eye of Figure 7 which points out the q-position where the Guinier regime starts. N_{PA_agg} decreases from ~ 30 for nanoparticles A (obtained by the same study as described in previous part) to a few nanoparticles for nanoparticles D. In this latter case, it is difficult to get N_{PA_agg} with a good accuracy because there is a large uncertainty on R_{NP_mean}. It is due to the cross-over of the Guinier Regime of the primary aggregate with the correlation peak corresponding to the contact between two nanoparticles (R_{PA_mean} is only almost 2 times R_{NP_mean} for nanoparticles D). The decrease of N_{PA_agg} while increasing R_{NP_mean} is nicely illustrated in Figure 7.b and in Figure 7.c that present TEM pictures of primary aggregates for both types of nanoparticles A and D.
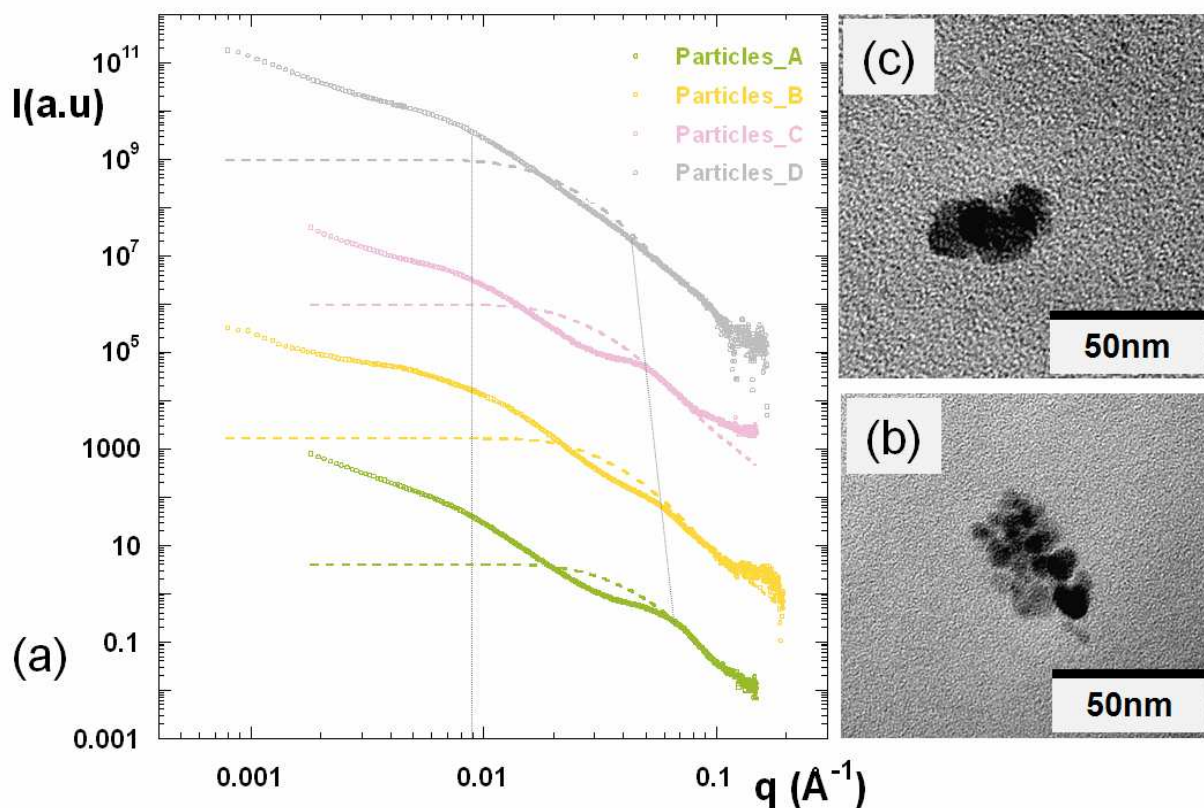
Figure 7: Influence of the nanoparticles' size on the structure of primary aggregates. (a) Comparison of SAXS spectra for the different nanoparticles batches compared with their form factor. The scattering curves are shifted in intensity for clarity. The dashed lines correspond to the form factor of the nanoparticles. The two grey lines are only guides for the eyes that point out the q-position of the Guinier regime starts and the correlation peak corresponding to the contact between two nanoparticless. (b) TEM picture of a nanocomposite made of nanoparticles A at $\Phi_{mag} = 10^{-5}$. (c) TEM picture of a nanocomposite made of nanoparticles D at $\Phi_{mag} = 10^{-5}$.

Figure 8.a presents the influence of the nanoparticles size on the structure of supra-aggregates, by comparing the SAXS scattering spectra of the four samples made at $\Phi_{mag} = 5.10^{-4}$. At very low q (besides the structure of the primary aggregates), all the scattering curves are exactly the same, as highlighted Figure 8.b where all the experimental scattering curves are rescaled in intensity. Figure 8.d to Figure 8.g present TEM pictures of supra-aggregates for both types of nanoparticles A and D at Φ_{mag}

= 5.10^{-4} for two different magnifications. For the 4 nanoparticles sizes, the samples form exactly the same kind of supra-aggregate made of primary aggregates of the same mean radius.
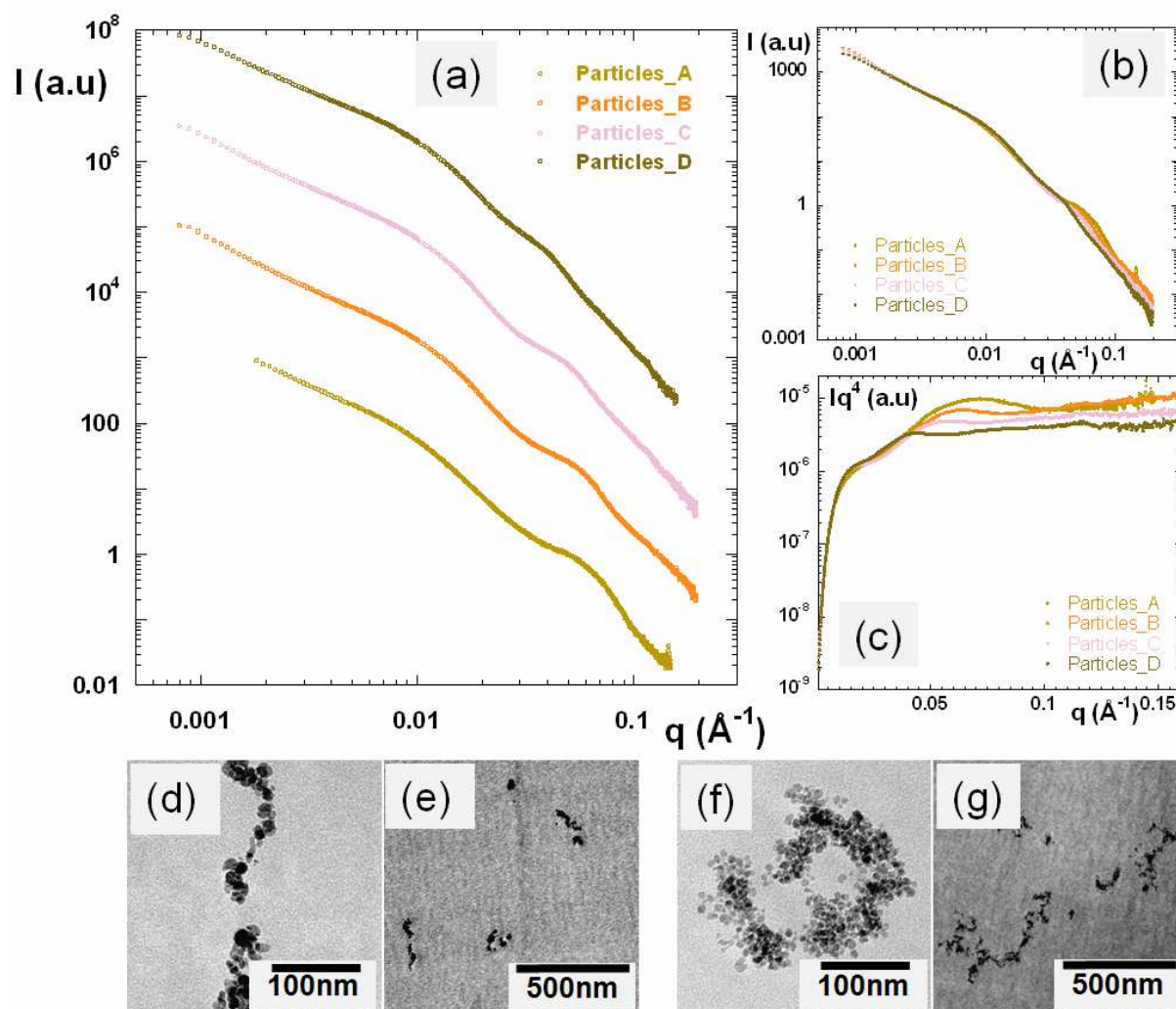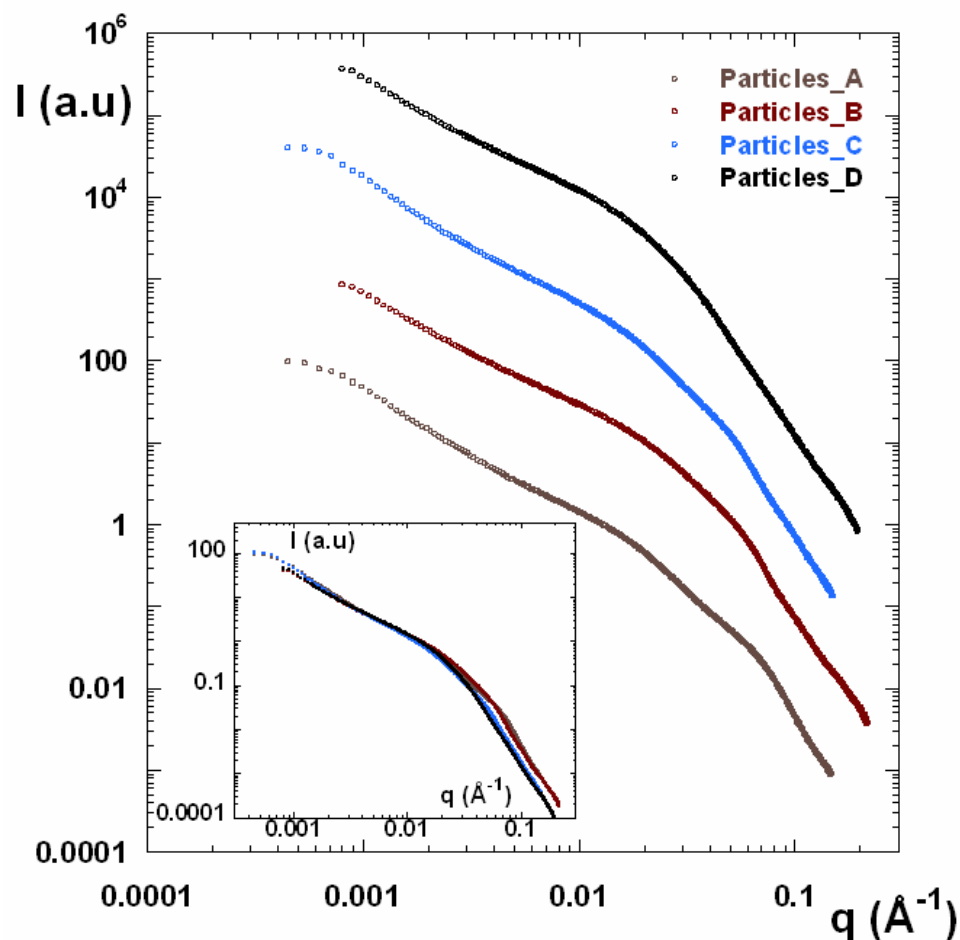

Figure 8: Influence of the nanoparticles' size on the structure of supra-aggregates. (a) Comparison of SAXS spectra for the different nanoparticles batches at $\Phi_{mag} = 5.10^{-4}$. The scattering curves are shifted in intensity for clarity. (b) Same scattering curves rescaled in intensity to the one of nanoparticles A. (c) $q^4 I(q)$ versus q for the same scattering curves. (d) & (e) TEM pictures of a nanocomposite made of nanoparticles D at $\Phi_{mag} = 5.10^{-4}$ at different magnifications. (f) & (g) TEM picture of a nanocomposite made of nanoparticles A at $\Phi_{mag} = 5.10^{-4}$ at different magnifications.

The modification of the specific surface of the primary aggregates with the particles' size resulting from the variation of the number of the native nanoparticles per primary aggregate is illustrated in the $I.q^4$

30

versus q representation of figure 8.c. At large q in the so-called limiting Porod regime, all the curves exhibit a plateau, of which intensity is directly proportional to the S/V ratio of the aggregates. This intensity nicely decreases when the nanoparticles' size increases. This means that the contact surface between the polymer matrix and the filler, i.e. the quantity of chains influenced by the proximity of the filler, can be easily tuned by the native nanoparticles' size without modifying the surface of the nanoparticles and thus the nature of the interaction with the polymer.

Figure 9 displays the SAXS scattering curves of the nanocomposites made at a higher concentration (Φ_{mag} = 0.03), in the regime where the supra-aggregates are close to the percolation threshold, for the four nanoparticles's size. The previous analysis is confirmed as presented in the inset of Figure 8 where all the experimental scattering curves are rescaled in intensity. They perfectly superimpose together, indicating that all the samples have the same structure in this q-range.

Figure 9: Influence of the nanoparticles' size on the structure of supra-aggregates. Comparison of SAXS spectra for the different nanoparticles batches at Φ_{mag} = 0.03. The scattering curves are shifted in intensity for clarity. Inset: Same scattering curves rescaled in intensity to the one of nanoparticles A

4 Mechanisms of formation of the primary aggregates and of the supra-aggregates

We discuss here about the mechanisms of formation of supra-aggregates, in spite of the fact that they remain partially poorly understood. A full understanding would require the determination of the evolution of the structure of the system at different steps during the evaporation process, which is very difficult because it is not possible to match the signal from the remaining solvent in SAXS and it is not possible to get a good statistics at very low Φ_{mag} in SANS. However, the amount of reproducible structural data obtained here on the system allows us to reveal some major trends to describe them.

First, the aggregation of the nanoparticles occurs during the film processing, only after the beginning of the DMAc evaporation. As proven by the results of part III.2, there are still repulsions between the naked γ-Fe_2O_3 nanoparticles when they are mixed with PS chains in DMAc. A mechanism of initial aggregation of the nanoparticles induced by the PS chains can thus be dismissed.

Second, the aggregation mechanism during drying is a two-step process. As the primary aggregates are obtained in a reproducible way for all the samples at Φ_{mag} down to 10^{-5}, they are presumably formed during an initial step of the drying. For the concentrated samples, a secondary step of aggregation, which leads to supra-aggregates, should occur only later during the drying process.

The primary aggregation step process is unexpected, and its mechanisms of formation remain unclear. It does not come from direct interactions between nanoparticles because this aggregation step occurs even at Φ_{mag} down to 10^{-5} after drying. For $\Phi_{mag} = 10^{-5}$, the mean distance between two nanoparticles d_{mean} in the initial homogeneous dispersion of spheres is higher than $(d_{NP\_mean})\sqrt[3]{\dfrac{\pi}{6 \cdot 10^{-5}}}$ where d_{NP_mean} is

the mean diameter of the nanoparticles. Thus $d_{mean} > \sim 40\ d_{NP\_mean}$. For electrostatic suspensions of maghemite nanoparticles of such a typical diameter, it has been shown in [Cousin 2003] that the interparticle potential between nanoparticles almost vanish at $d_{mean} \sim 3\ d_{NP\_mean}$ because all the interactions have a limited range (Van der Waals attractions, magnetic dipolar attractions and electrostatic repulsions). Some eventual depletion interactions induced by the PS chains have also a very limited range (see part III.2). Moreover, an aggregation process driven by such attractive interactions would have lead to an increase of N_{PA_agg} with R_{NP_mean}, but the opposite effect is observed. As the primary aggregation leads to clusters which always have roughly the same size, the understanding of its origin may pass through the identification of the parameter of our experimental system that has such a characteristic size ($\sim$ 168 Å). This is not the mean radius of the nanoparticles R_{NP_mean}. It is much closer to the gyration radius of the PS chains in θ solvent used here (we get 230 Å for PS chains of M_w 280 000 g/mol). However the PS chains are in semi-dilute regime before casting with a characteristics blob size ξ of 11Å [32], a size much lower than the one of the primary aggregates. It is likely that for nanoparticles of higher mean radius, the primary aggregation step would disappear.

The secondary aggregation step process, that leads to open fractal aggregates with a D^f of 1.7, is much easier to understand. This fractal dimension is indeed very close to 1.78, corresponding to the one measured and computed [33] for colloids aggregated through a Diffusion Limited Aggregation (DLA) process. As primary aggregates do not interact a priori, their further aggregation can thus only be driven by diffusion processes. Theses processes are progressively frozen during drying, because the viscosity diverges. They do not occur for very dilute systems, because the primary aggregates are too far away from each other to aggregate by DLA before freezing. Once a critical concentration of primary aggregates is reached (ranging from $\Phi_{mag} = 10^{-4}$ to $5\ 10^{-4}$), the system becomes concentrated enough in primary aggregates to allow DLA processes. The aggregation is limited at much larger scale by the competing effects of both the increase of the aggregates size by the DLA and of the freezing of the system, which leads to the finite size of supra-aggregates. As Φ_{mag} has a minor impact on the viscosity of the whole mixture, the process is similar for all samples, and leads to the same size.

5 Specificity of the system

If some mechanisms of formation of the supra-aggregates remain to be understood, the clear description of the final dispersion of the maghemite nanoparticles inside the PS matrix gives an original picture. To our best knowledge, a reproducible two-step aggregation process of native nanoparticles inside a polymer matrix has never been reported in the literature on comparable systems (naked nanoparticles mixed with polymer chains). The formation of nanocomposites is usually driven by a more classical single-step aggregation process [5,34, 35] The native particles form objects of finite size at low content which percolate when increasing the concentration.

This original two-step process, associated to the possibility of tuning the polymer-filler surface contact by the size of the native particles, is a very promising way to understand the microscopic mechanisms of the mechanical properties of reinforced materials, which involve two contributions in the elastic modulus, one coming from the fillers and one coming from the polymer chain. It is actually difficult to discriminate from an experimental point of view these two contributions. Indeed, changing the polymer-filler interaction in order to probe the chain contribution usually modifies also the filler organization. Reciprocally, changing the filler structure, for example by the particles' concentration, also modifies the polymer-filler interactions.

To date, some fillers effects have been clearly described in the literature, especially the deviation of the hydrodynamic reinforcement associated to the percolation process of the fillers [Heinrich 2002]. But some other effects below the percolation threshold, like the existence of an elastic contribution, have been also observed [36]. The origin of this last contribution, which involves both the conformation [37] and the dynamic [12] of some polymer chains in the vicinity of the filler, is still under discussion. It remains indeed difficult to highlight it directly because it depends on the fraction of the implicated chains, which is difficult to evaluate and could be reduced to a small value [13]. Thus, our experimental system is of great interest to understand the contribution of the polymer chains in the mechanical

reinforcement because it enables to increase the fraction of the implicated chains by changing the specific surface of the fillers without changing the fillers contributions (the threshold percolation, here, is mainly related to the size of the supra-aggregates and it is independent of the size of the native maghemite nanoparticles).

V Conclusion and perspectives

We have shown here first how we have succeeded in obtaining stable colloidal suspensions of magnetic nanoparticles of maghemite (γ-Fe$_2$O$_3$) of ~ 40 Å of radius in dimethylacetamide (DMAc), a polar solvent which is also a good solvent of several common polymer chains (PS, PMMA, …). This was obtained by a gentle exchange of solvents by dialysis on suspensions that were initially synthetized in water, without any treatment of the bare nanoparticles. Such suspensions are promising from a polymer science point of view, as they could be the starting point of controlled polymerizations from the surface of the nanoparticles while keeping colloidal stability to achieve PS-grafted nanoparticles with controlled corona. Several successful polymerizations from different "Grafting from" routes have been reported on close systems made of silica nanoparticles stabilized in DMAc (ATRP [38], NMP [15]).

We have also shown that we were able to easily produce highly reproducible nanocomposites made of such γ-Fe$_2$O$_3$ nanoparticles dispersed in a polystyrene matrix. At high volume fraction ($\Phi_{mag} \geq 5 \ 10^{-4}$), the magnetic nanoparticles in the matrix were forming an homogeneous dispersion of supra-aggregates with a finite size of around ~ 200 nm, with a hierarchical structure made of dense primary aggregates composed of some tens of nanoparticles. The latter supra-aggregates are organized in fractal way at higher scale with a dimension of 1.7. At low volume fraction ($\Phi_{mag} \leq 10^{-4}$), only the primary aggregates were obtained. All the structural parameters of the supra-aggregates were perfectly characterized by an analysis combining SAXS and TEM microscopy.

A remarkable specificity of the system comes from the reproducibility of the hierarchical structure obtained at a large scale. It is indeed possible to tune the inner structure of the elementary 'bricks'

35

forming the supra-aggregates (the primary aggregates) by an appropriate choice of the initial size of the nanoparticles without altering the structure at larger scale. This provides huge potentials to the system that will be presented in forthcoming studies:

(i) First, it is a perfect model system to go further in the understanding of mechanical properties of nanocomposites because it allows to uncouple perfectly the respective contribution of the filler structure and polymer dynamics to the reinforcement. It allows indeed to process different samples with the same filler structure and the same Φ_{SA}, either below the percolation threshold or above it, but with different surface contact between the nanoparticles and the PS matrix by playing on the nanoparticles' size.

(ii) Second, the primary aggregates are a powerful tool to design new nanocomposites with various and controlled anisotropic morphologies of the filler, ranging from slightly anisotropic structures to highly anisotropic structures. This can be done by using an external magnetic field during casting and playing on the magnetic susceptibility of the nanoparticles, that strongly increases with the size of the nanoparticles.

Supporting Information Available. The magnetization curves of supensions of $\gamma-Fe_2O_3$ magnetic nanoparticles in H_2O, the SAXS spectra of suspensions of $\gamma-Fe_2O_3$ magnetic nanoparticles in H_2O and the SAXS spectra of $\gamma-Fe_2O_3$ nanoparticles in the nanocomposites polymeric films are presented in Supporting Information. This material is available free of charge via the Internet at http://pubs.acs.org.

References

[1] Vaia, R. A.; Maguire, J. F. *Chem. Mater.* **2007,** *19,* 2736-2751

[2] Tjong, S. C. *Materials Science and Engineering*, **2006**, 73-197.

[3] Guth, E.; Gold, O. *Phys. Rev.*, **1938**, *53*, 322.

[4] Heinrich, G.; Kluppel, M.; Vilgis, T. A *Current Opinion Solid State and Materials Science,* **2002***, 6*, 195–203.

[5] Jouault, N.; Vallat, P.; Dalmas, F.; Said, S.; Jestin, J.; Boué, F. *Macromolecules* **2009**, *42(6)*, 2031–2040.

[6 Botti, A.; Pyckout-Hintzen, W.; Richter, D.; Urban, V.; Straube, E. *J. Chem. Phys.* **2006**, 124.

[7] Kropka, J. M.; Putz, K. W.; Pryamitsyn, V.; Ganesan, V.; Green, P. F. *Macromolecules* **2007**, 40, 5424-5432.

[8] Rharbi, Y.; Cabane, B.; Vacher, A.; Joanicot, M.; Boué, F. *Europhys. Letters,* **1999***, 46*, 472-478.

[9] Mark, J. E.; Abou-Hussein, R.; Sen, T. Z.; Kloczkowski, A. *Polymer,* **2005***, 46*, 8894-8904

[10] Tuteja, A.; Duxbury, P. M.; Mackay, M. E. *Phys. Rev. Letters,* **2008***, 100*, 077801.

[11] Nakatani, A. I.; Chen, W.; Schmidt, R. G.; Gordon, G. V.; Han, C. C. *Polymer,* **2001***, 42,* 3713-3722.

[12] Long, D.; Lequeux, F. *Europhys. Letters*, **2001**, 4, 371.

[13] N. Jouault, F. Dalmas, S. Said, E. Di-Cola, R. Schweins, J. Jestin, F. Boué, *2010*, Submitted.

[14] Akcora, P.; Liu, H.; Kumar, S. K. ; Moll, J.; Li, Y.; Benicewicz, B. C. ; Schadler, L. S. ; Acehan, D. ; Panagiotopoulos, A. Z. ; Pryamitsyn, V.; Ganesan, V.; Ilavsky, J. ; Thiyagarajan, P.; Colby, R. H. ; Douglas, J. *Nat. Mater.*, **2009**, *8*, 354-359

[15] Chevigny, C.; Gigmes, D.; Bertin, D.; Jestin, J., Boué, F. *Soft Matter*, **2009**, 5(19), 3741-3753.

[16] Dalmas, F.; Cavaillé, J.-Y.; Gauthier, C. ; Chazeau, L.; Dendievel, R. *Compos. Sci. Technol.,* **2007**, *67*, 829–839.

[17] Oberdisse, J.; El Harrak, A.; Carrot, G.; Jestin, J.; Boué, F. *Polymer,* **2005**, *46*, 6695–6705

[18] Massart, R.; Dubois, E.; Cabuil, V. ; Hasmonay, E. *J. Magn. Magn. Mater.* **1995**, *149*, 1-5.

[19] E. Dubois, E.; Perzynski, R.; Boué, F.; Cabuil, V. *Langmuir*, **2000**, *16(13)*, 5617-5625.

[20] Varga, Z.; Filipcsei, G.; Zrinyi, M. *Polymer*, **2006**, *47*, 227.

[21] Galicia, A.; Cousin, F.; Cabuil, V.; Dubois, E.; Sandre, O.; Perzynski, R. *Soft Matter,* **2009**, *5*, 2614-2624.

[22] Jestin, J.; Cousin, F.; Dubois, I.; Ménager, C.; Oberdisse, J.; Schweins, R.; Boué, F. *Adv. Mater.,* **2008**, *20(13)*, 2533-2540.

[23] Massart, R. *I.E.E.E. Trans. Magn.* **1981**, *17*, 1247

[24] *Magnetic Fluids and Applications Handbook*, ed. by B. Berkovski (Begell House Inc. Publ., New York, 1996.

[25] Brûlet, A.; Lairez, D.; Lapp, A.; Cotton, J.-P. *J. Appl. Cryst.* **2007**, *40*, 165–177

[26] Cousin, F.; Cabuil, V. *J. Mol. Liq.* **1999**, *83*, 203-215.

[27] Cousin, F.; Dubois, E.; Cabuil, V. *Phys. Rev. E*, **2003**, 68(2), 021405

[28] Israelachvili, J. *Intermolecular and Surface Forces*, Academic Press, New York, **1992**.

[29] Scaling concepts in polymer physcics

[30] Rottler, J.; Robbins, M. O. *Phys. Rev. E*, **2003**, *68(1)*, 011801.

[31] Fresnais, J.; Berret, J.-F.; Qi, L. ; Chapel, J.-P.; Castaing, J.-C.; Sandre, O.; Frka-Petesic, B.; Perzynski, R. ; Oberdisse, J.; Cousin, F. *Phys. Rev. E* **2008**, *78*, 040401.

[32] De Gennes, P.G. *Scaling Concepts in Polymer Physics*; Cornell University Press: Ithaca, NY, **1979**.

[33] Lin, M. Y.; Lindsay, H. M.; Weitz, D. A.R.; Ball, C. ; Klein, R. ; Meakin, P. *Phys. Rev. A* **1990**, *41*, 2005.

[34] Bansal A.; Yang, H.; Li, C.; Cho, K.; Benicewicz, B. C.; Kumar, S. K.; Schadler, L. S. *Nat. Mater.* **2005**, *4*, 693-698.

[35] Sen, S. ; Xie, Y.; Bansal, A.; Yang, H.; Cho, K.; Schadler, L. S.; Kumar, S. K. *Eur. Phys. J. Spec. Top.* **2007**, *141*, 161–165.

[36] Tsagaropoulos, G.; Eisenberg, A. *Macromolecules* **1995**, *28*, 6067–6077.

[37] Sarvestani, A. S. *Eur. Polym. J.* **2008**, *44*, 263–269.

[38] Carrot, G.; El Harrak, A.; Oberdisse, J.; Jestin, J. ; Boué, F. *Soft Matter*, **2006**, *2(12)*, 1043-1047.

Homogeneous Dispersion of Magnetic Nanoparticles Aggregates in a PS Nanocomposite: Highly Reproducible Hierarchical Structure tuned by the Nanoparticles' Size.

Anne-Sophie Robbes[1,2], Jacques Jestin[1], Florian Meneau[2], Florent Dalmas[3], Olivier Sandre[4], Javier Perez[2], François Boué[1], Fabrice Cousin[1,]*

[1]Laboratoire Léon Brillouin, CEA Saclay 91191 Gif sur Yvette, Cedex France

[2]Synchrotron SOLEIL L'Orme des Merisiers, PO Box 48, Saint-Aubin, 91192 Gif sur Yvette, France

[3]Institut de Chimie et des Matériaux Paris-Est, CNRS UMR 7182, 2-8 rue Henri Dunant 94320 Thiais, France

[4]Laboratoire Physicochimie des Electrolytes, Colloïdes et Sciences Analytiques, UMR CNRS-UPMC-Univ Paris 6-ESPCI-Paris Tech 7195, 4 place Jussieu, case 51, 75005 Paris, France

[*] Corresponding author: fabrice.cousin@cea.fr

1 SAXS spectra of suspensions of γFe_2O_3 magnetic nanoparticles in H_2O and DMAc
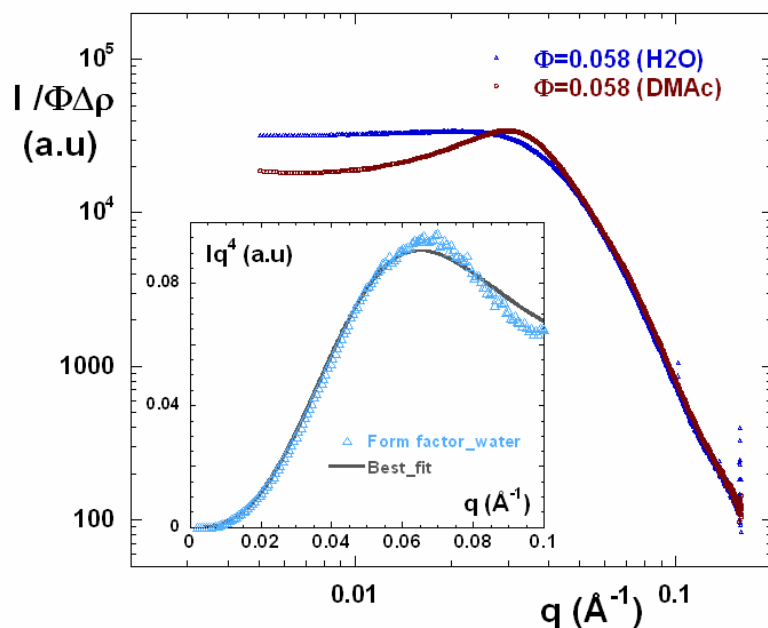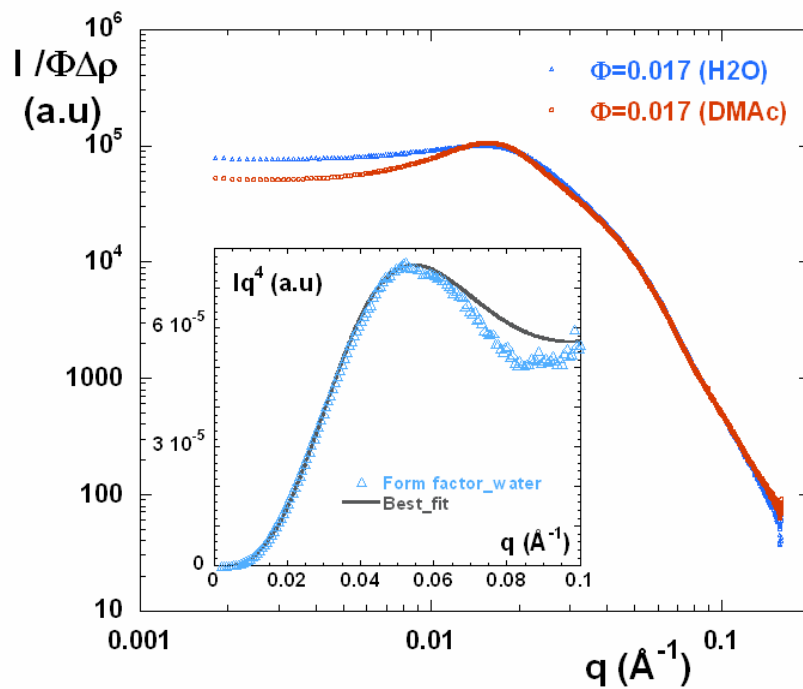

Figure SI 1.a: SAXS scattering curves for the suspensions of nanoparticles A either in water or in DMAc presented in a $I(q)/\Phi\Delta\rho = f(q)$ representation. $\Delta\rho$ stands either for $(\rho_{mag} - \rho_{DMAc})^2$ or $(\rho_{mag} - \rho_{water})^2$ depending on the solvent used. Inset: $q^4 I(q)$ versus q for $\Phi_{mag} = 0.001$ in water. The full line corresponds to the best fit of the form factor.
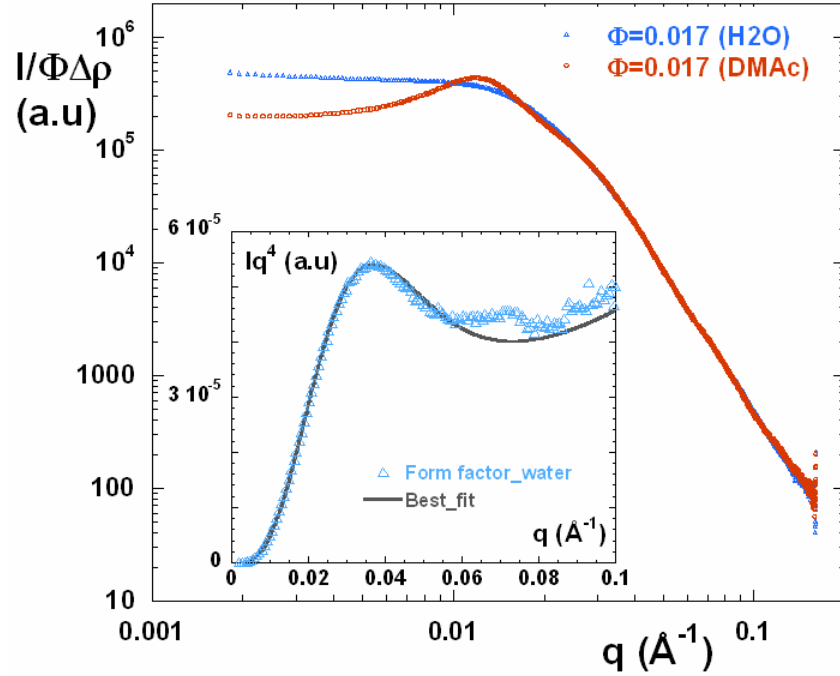
Figure SI 1.b: SAXS scattering curves for the suspensions of nanoparticles B either in water or in DMAc presented in a $I(q)/\Phi\Delta\rho = f(q)$ representation. $\Delta\rho$ stands either for $(\rho_{mag} - \rho_{DMAc})^2$ or $(\rho_{mag} - \rho_{water})^2$ depending on the solvent used. Inset: $q^4 I(q)$ versus q for $\Phi_{mag} = 0.001$ in water. The full line corresponds to the best fit of the form factor.

Figure SI 1.c: SAXS scattering curves for the suspensions of nanoparticles D either in water or in DMAc presented in a $I(q)/\Phi\Delta\rho = f(q)$ representation. $\Delta\rho$ stands either for $(\rho_{mag} - \rho_{DMAc})^2$ or $(\rho_{mag} - \rho_{water})^2$ depending on the solvent used. Inset: $q^4 I(q)$ versus q for $\Phi_{mag} = 0.001$ in water. The full line corresponds to the best fit of the form factor.

2 Magnetization curves of suspensions of γFe_2O_3 magnetic nanoparticles in H_2O

In order to determine the volume fraction of the different suspensions after synthesis and the size distribution of the nanoparticles, we have measured the magnetization curves of the suspensions in H_2O.

We briefly recall the principle here. Each nanoparticle bears a magnetic moment $\vec{\mu}$ which is of the order of 10^4 Bohr magnetons. Its modulus $|\vec{\mu}| = m_S V_{magn}$ is proportional to the magnetic volume V_{magn} of the nanoparticles and to m_S the magnetization of the maghemite. Under a large applied field $\vec{H}$, this magnetic moment $\vec{\mu}$ orientates along the field direction. In a liquid suspension of γ-Fe_2O_3 nanoparticles of radius ~ 4 nm, it also rotates mechanically the core of the nanoparticle. The alignment of $\vec{\mu}$ along $\vec{H}$ provides to the suspension a

macroscopic magnetization M. At saturation, all the magnetic moments align along $\vec{H}$, then M = M_S = $m_S\Phi$. For intermediate fields, the behavior of the suspension is superparamagnetic. For a suspension of monodisperse nanoparticles of radius R, M is well described by the first Langevin law L(R) at low Φ (when dipole-dipole correlations are neglected) :

$$M(H) = M_S(\coth\frac{\mu_0\mu H}{kT} - \frac{kT}{\mu_0\mu H}) \quad \text{with } M_S = m_s\Phi \tag{1}$$

For polydisperse suspensions, the shape of the curves M(H) is modified by the log-normal size distribution of the particles size P(R0, s) (see equation 2 of main text) :

$$\frac{M(H)}{M_S}(R_0,\sigma) = \frac{\int_0^\infty d^3 P(R)L(R,H)dR}{\int_0^\infty d^3 P(R)dR} \tag{2}$$

At low H, in the linear regime, the magnetization curve is proportional to the magnetic susceptibility of the nanoparticles. The magnetization curves are presented for the different batches of nanoparticles A, B, C and D in Figure SI.1.
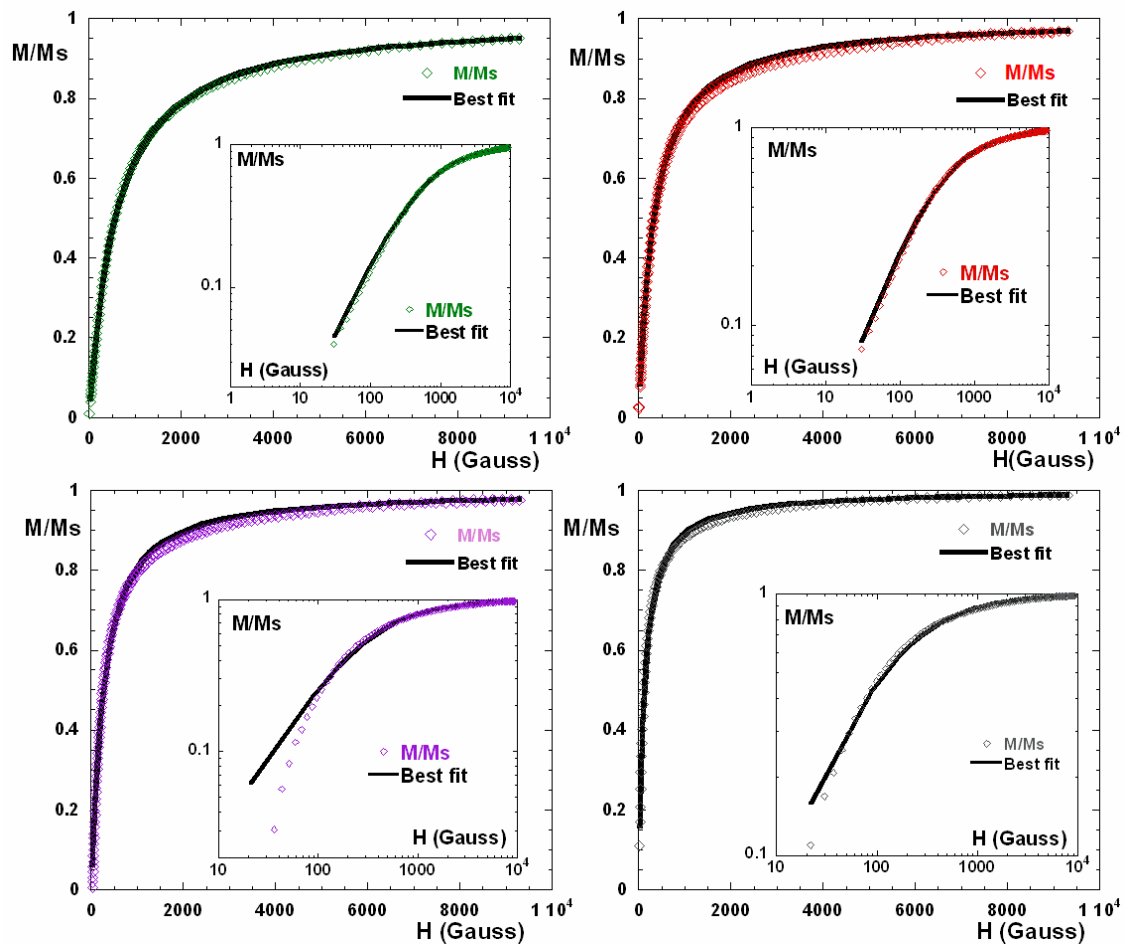
Figure SI.2: Magnetization curve of the suspensions of γFe_2O_3 nanoparticles in H_2O. The magnetization curves are modelled by the first Langevin law and take into account the polydispersity of the nanoparticles. Inset: same curves in log-log scale. (a) batch A; (b) batch B; (c) batch C; (d) batch D.

3 SAXS spectra of γFe₂O₃ nanoparticles in the nanocomposite polymeric films

Figure SI.3.a: SAXS scattering curves of the γFe₂O₃ nanoparticles in the PS polymeric matrix obtained by SAXS for nanoparticles A. The dashed lines correspond to the form factor of the nanoparticles.
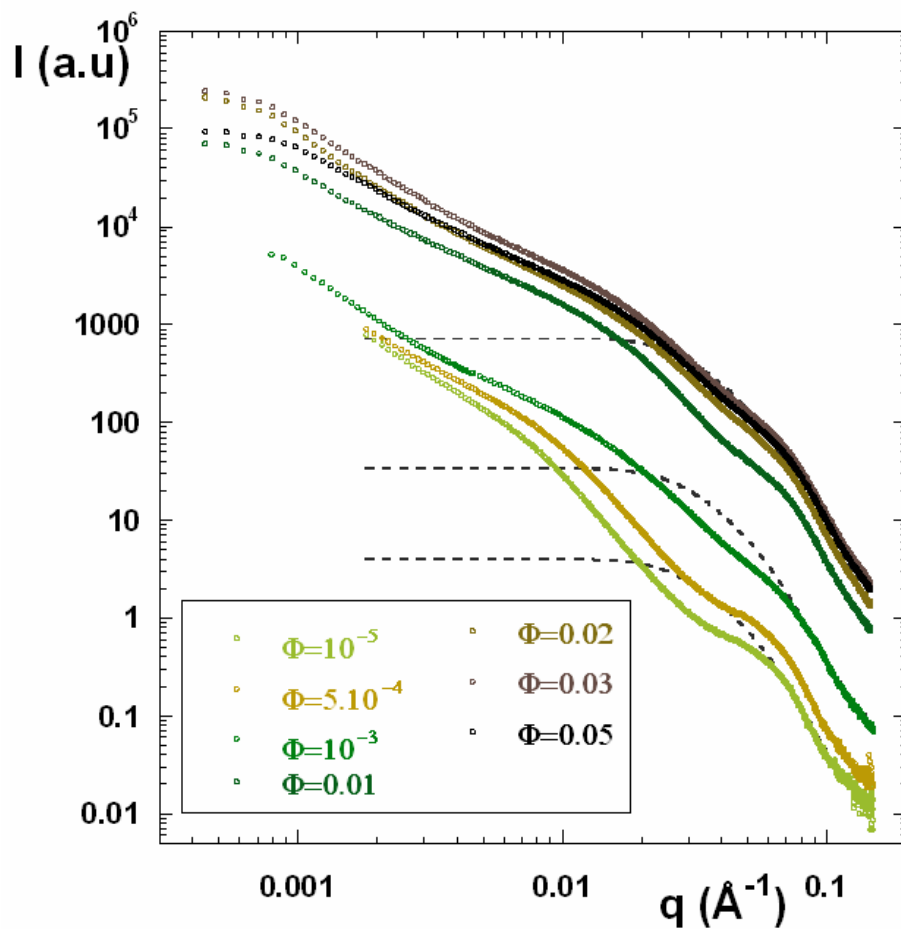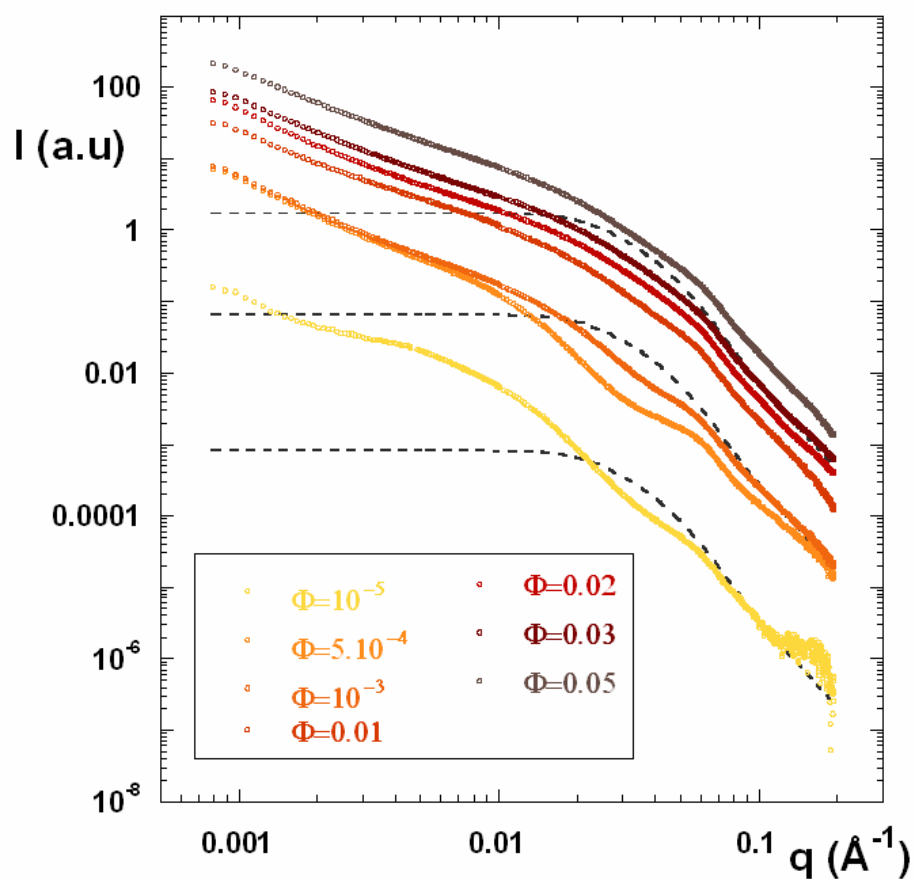
Figure SI.3.b: SAXS scattering curves of the γFe_2O_3 nanoparticles in the PS polymeric matrix obtained by SAXS for nanoparticles B. The dashed lines correspond to the form factor of the nanoparticles.
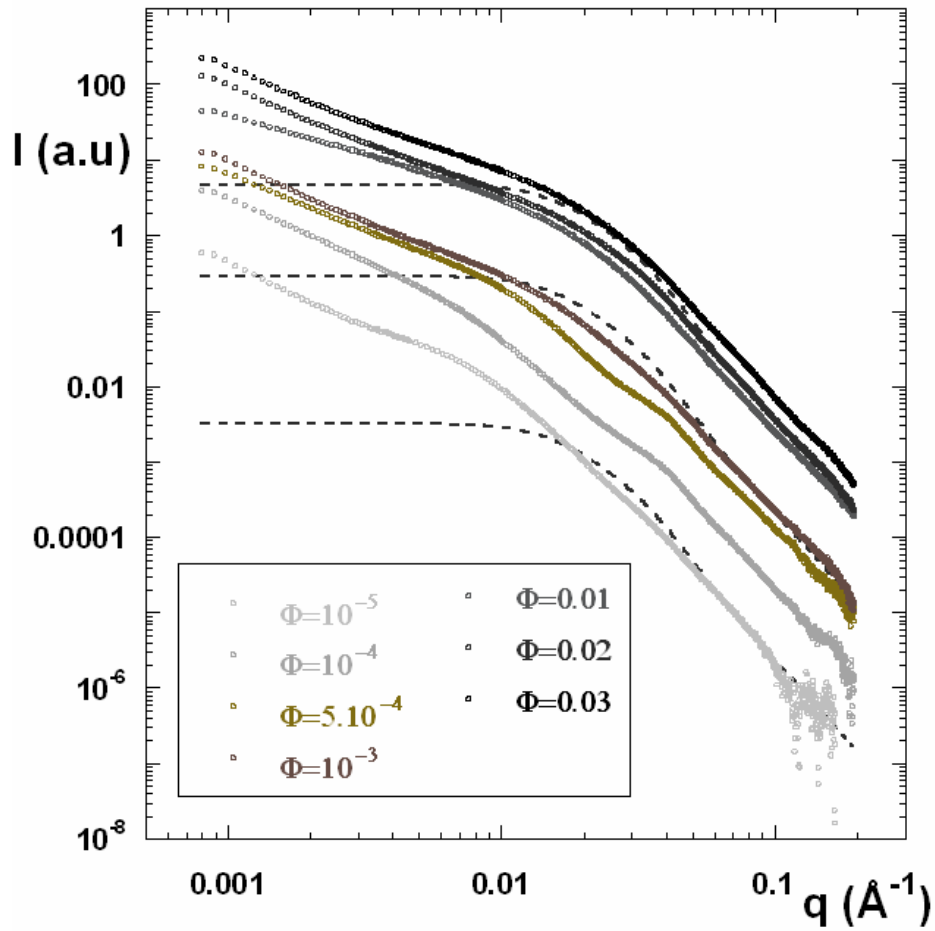
Figure SI.3.c: SAXS scattering curves of the γFe_2O_3 nanoparticles in the PS polymeric matrix obtained by SAXS for nanoparticles D. The dashed lines correspond to the form factor of the nanoparticles.